CANMET

REPORT 80-1

Canada Centre for Mineral and Energy Technology

Centre canadien de la technologie des minéraux et de l'énergie

SODIUM BETA- AND BETA"-ALUMINA CERAMICS: POWDER PREPARATION

D.J. GREEN AND T.A. WHEAT

ENERGY RESEARCH PROGRAM

MINERAL SCIENCES LABORATORIES

Energy, Mines and Resources Canada

Énergie, Mines et Ressources Canada

MAY 1980

Available in Canada through

Authorized Bookstore Agents
and other bookstores

or by mail from

Canadian Government Publishing Centre
Supply and Services Canada
Hull, Quebec, Canada K1A 0S9

CANMET
Energy, Mines and Resources Canada,
555 Booth St.,
Ottawa, Canada K1A 0G1

or through your bookseller

Catalogue No. M38–13/80-1E
ISBN 0-660-10655-8

Canada: $2.95
Other countries: $3.55

Price subject to change without notice.

En vente au Canada par l'entremise de nos

agents libraires agréés
et autres librairies

ou par la poste au:

Centre d'édition du gouvernement du Canada
Approvisionnements et Services Canada
Hull, Québec, Canada K1A 0S9

CANMET
Énergie, Mines et Resources Canada,
555, rue Booth
Ottawa, Canada K1A 0G1

ou chez votre libraire.

Nº de catalogue M38–13/80-1E
ISBN 0-660-10655-8

Canada: $2.95
Hors Canada: $3.55

Prix sujet à changement sans avis préalable.

SODIUM BETA- AND BETA"-ALUMINA CERAMICS: POWDER PREPARATION

by

D.J. Green* and T.A. Wheat*

ABSTRACT

The present work forms part of a program to develop ionically conducting materials for potential use in energy storage and conversion systems. With applications in high energy-density batteries, high temperature thermoelectric generators, fuel cells and sensors, they are playing an increasingly important role in the development of more efficient energy storage and conversion devices.

Of the many solid-state cationic conductors known, the most widely studied at present are those occurring in the system Na_2O-Al_2O_3 in which occur the two forms: beta-alumina (nominally $Na_2O.11Al_2O_3$) and the more conductive beta"-alumina (nominally $Na_2O.6Al_2O_3$). Because of the practical importance of these sodium-conducting materials in future energy systems, a program was initiated in CANMET to study the relationship between the various processing parameters and the properties of the final sintered product. To minimize contamination and other extrinsic effects, the materials were prepared using wet chemical techniques.

Powders of sodium beta/beta"-alumina were prepared by the techniques of solution spray freezing-freeze drying and solution spray drying. After drying, powders were in the form of spheres with the physical structure of these spheres depending on the drying process. The powders were found to have high surface areas after decomposition and to form a mixture of the beta and beta" phases at ~1250°C. During calcination there is a tendency for the powders to agglomerate but the spherical nature of the dried powder still persists. The calcined spheres were found to be complex aggregates of very fine crystals. The powders were shown to be prone to sodium loss at temperatures above ~1300°C.

---

*Research scientist, Ceramics Section, Industrial Minerals Laboratory, Mineral Sciences Laboratories, CANMET, Energy, Mines and Resources Canada, Ottawa.

LES CERAMIQUES DE SODIUM D'ALUMINE BETA ET BETA": PREPARATION DE LA POUDRE

par

D.J. Green* et T.A. Wheat*

RESUME

Le présent travail a été effectué dans le cadre d'un programmme de mise au point des matériaux à conduction ionique pour l'usage possible dans les systèmes d'emmagasinage et de conversion de l'énergie. Comme on peut les utiliser dans les piles à haute densité d'énergie, dans les génératrices themoélectriques à haute température, dans les piles à combustibles et dans les sondes, ces matériaux jouent un rôle de plus en plus important dans la mise au point de dispositifs plus efficaces pour l'emmagasinage et la conversion de l'énergie.

Des nombreux conducteurs cationiques à l'état solides connus, ceux qui jusqu'à présent ont été les plus étudiés sont ceux que l'on retrouve dans le système Na_2O-Al_2O_3 dans lequel se trouvent les deux formes suivantes: le bêta-alumine ($Na_2O.11Al_2O_3$) et le bêta"-alumine plus conducteur ($Na_2O.6Al_2O_3$). A cause de l'importance pratique de ces matériaux conducteur de sodium pour les systèmes d'énergie futurs, un programme a été lancé au CANMET pour étudier le rapport qui peut exister entre les différents paramètres de transformation et les propriétés du produit concrétionné fini. Les matériaux ont été préparés selon des techniques chimiques humides afin de minimiser la contamination et autres effets intrinsèques.

Les poudres d'alumine bêta et bêta" de sodium ont été préparées selon les techniques de gel par la vaporisation de solution-séchage par le gel et le séchage par la vaporisation d'une solution. Après le séchage, les poudres prenaient la forme de sphères. La structure physique de ces sphères dépend du procédé de séchage. Les poudres ont des grandes aires de surface après la décomposition et forment un mélange des phases bêta et bêta" à ∿1250°C. Durant la calcination, la poudre a tendance à s'agglomérer mais la nature sphérique de la poudre séchée persiste. On a découvert que les sphères calcinées sont des agrégats complexes de cristaux très fins. On a démontré que ces poudres étaient sujets à des pertes de sodium à des températures de plus de ∿1300°C.

---

*Chercheurs scientifiques, Section des céramiques, Laboratoire des minéraux industriels, Laboratoires des sciences minérales, CANMET, Energie, Mines et Ressources Canada, Ottawa.

CONTENTS

	Page
ABSTRACT	i
RESUME	ii
INTRODUCTION	1
LITERATURE SURVEY	1
Freeze Drying	6
Spray Drying	8
EXPERIMENTAL PROCEDURE	9
Solution Spray Freezing-Freeze Drying	9
Solution Spray Drying	9
Powder Characterization	9
RESULTS AND DISCUSSION	10
Freeze-Dried $Na_2O.6Al_2O_3$	10
Spray-Dried $Na_2O.6Al_2O_3$ (Sulphate Derived)	17
Spray-Dried $Na_2O.6Al_2O_3$ (Nitrate Derived)	24
CONCLUSIONS	26
Freeze-Dried $Na_2O.6Al_2O_3$	26
Spray-Dried $Na_2O.6Al_2O_3$ (Sulphate Derived)	27
Spray-Dried $Na_2O.6Al_2O_3$ (Nitrate Derived)	27
ACKNOWLEDGEMENTS	28
REFERENCES	28
APPENDIX A - X-RAY POWDER DIFFRACTION DATA FROM SODIUM BETA"-ALUMINA	A-33
APPENDIX B - X-RAY POWDER DIFFRACTION DATA FOR SODIUM BETA-ALUMINA	B-39

TABLES

1.	Phase sequence for freeze-dried powder	11
2.	X-ray diffraction pattern sodium beta"-alumina (Debye-Scherrer)	12
3.	X-ray diffraction pattern for sodium beta"-alumina (Guinier)	13
4.	Lattice parameters for sodium beta"-alumina (without stabilizer)	13
5.	Chemical analysis of freeze-dried powder	14
6.	Effect of concentration of specific surface area	17
7.	Phase sequence for calcined powders	19
8.	X-ray diffraction data for sodium β-Al_2O_3 (Debye-Scherrer)	20
9.	X-ray diffraction for Na β-Al_2O_3 (Guinier)	21
10.	Lattice parameters for Na β-Al_2O_3	21
11.	Spectrochemical analysis for calcined SD and FD powders (1300°C, 24 h)	22

CONTENTS (cont'd)

Page

Tables (cont'd)

12. Phase sequence of spray-dried nitrate powder compared with spray-dried sulphate powder 25

13. Specific surface area for spray-dried nitrate powder 26

14. Chemical analysis for spray-dried nitrate powder 26

A-1. Calculated X-ray powder diffraction pattern for sodium beta"-alumina A-35

B-1. Calculated X-ray powder diffraction pattern for sodium beta-alumina B-41

FIGURES

1. CANMET program on the preparation, fabrication and characterization of sodium beta- and beta"-alumina (Phase I) .. 1

2. Variation of sodium ion conductivity with temperature ... 2

3. Variation of resistivity with temperature in three samples of polycrystalline beta-alumina of the same composition but of different grain sizes 2

4. Crystal structures of sodium beta-alumina and sodium beta"-alumina 3

5. Section of Na_2O-Al_3O_3 pseudobinary phase diagram containing β and β"-alumina 4

6. Phase equilibria in the Na_2O-Al_2O_3 pseudobinary system 4

7. Phase equilibria in the $Al_2(SO_4)_3$-H_2O pseudobinary system 6

8. Schematic diagram of a commercial freeze drier 7

9. Phase equilibria in a salt-water system 7

10. Phase equilibria in the ternary system $Al_2(SO_4)$-Na_2SO_4 -H_2O 7

11. Typical conditions in a freeze drier during the sublimation (drying) stage 8

12. Schematic of a commercial spray drier 8

13. Optical micrograph of freeze-dried powder 10

14. Scanning electron micrograph of freeze-dried powder 10

15. Surface of freeze-dried sphere 10

16. X-ray diffraction pattern (after drying) 11

17. Ir spectrum of as-prepared powder obtained by freeze-drying a 1:6 sulphate solution 11

18. Debye-Scherrer X-ray diffraction pattern for Na β" - Al_2O_3 (CoKα radiation, Fe filter) 12

CONTENTS (cont'd)

Page

Figures (cont'd)

19. Guinier X-ray diffraction patterns for calcined phases .. 13

20. TBA for freeze-dried powder 13

21. DTA trace for freeze-dried powder 14

22. Specific surface area of freeze-dried powder calcined in air for 1 h at the temperatures indicated 14

23. Scanning electron micrograph of calcined freeze-dried powder (1250°C, 1 h) 15

24. Surface of calcined, freeze-dried sphere (1250°C, 1 h) .. 15

25. Electron micrograph of calcined freeze-dried powder 15

26. Electron micrograph of calcined freeze-dried powder (1250°C, 1 h) viewed in dark field 15

27. Electron micrographs of calcined freeze-dried powder (1250°C, 1 h) viewed in bright field 15

28. Dark field electron micrograph 15

29. Bright field electron micrograph 16

30. TGA of as-prepared powder after freeze drying at different shelf temperatures 16

31. DTA of as-prepared powder after freeze drying to the shelf temperatures indicated 16

32. TGA of freeze-dried powders derived from solutions of different concentration 17

33. Optical micrograph of spray-dried powder viewed under crossed polars 17

34. Crushed spray-dried powder 18

35. SEM micrographs of spray-dried powder, as-dried and lightly crushed 18

36. Freeze-dried sphere 18

37. Structure within freeze-dried sphere 18

38. Comparison of X-ray diffraction patterns for FD and SD powders (calcined 1300°C, 1 h) 20

39. TGA for spray-dried (SD) and freeze-dried (FD) powders .. 21

40. TGA for spray-dried (SD) and Freeze-dried (FD) powders .. 21

41. DTA of freeze-dried powder 21

42. DTA of spray-dried powder 22

43. Specific surface area developed in spray-dried and freeze-dried powders on calcination for 1 h in air 22

44. Variation of the Al:Na mole ratio and total S content for spray-dried and freeze-dried materials resulting from calcination in air for 1 hr 22

CONTENTS (cont'd)

Page

Figures (cont'd)

45. IR spectrum of freeze-dried powder after calcination in air at 1300°C for 24 h 23

46. IR spectrum of spray-dried powder after calcination in air at 1300°C for 24 h 23

47. Calcined FD spheres (agglomerated) 23

48. Calcined FD sphere 23

49. Fine, equiaxed crystals formed in FD sphere 23

50. Formation of needle-shaped crystals within FD sphere 23

51. Crushed calcined FD powder 24

52. Calcined SD powder 24

53. Spray-dried powder (nitrate solution) viewed in reflected polarized light 25

54. SEM micrograph of spray-dried powder (nitrate solution) . 25

55. SEM micrograph of spray-dried powder (nitrate solution) showing the presence of hollow spheres 25

56. TGA of spray-dried powder derived from nitrate solution . 26

57. DTA of spray-dried powder derived from nitrate solution . 26

58. SEM micrographs of spray-dried powder derived from a nitrate solution and calcined in air at 1350°C 27

INTRODUCTION

Although it has been known for some time that certain solids were capable of conducting electricity by ionic transport, it is only within the last 20 years that the scientific significance of these solid-state electrolytes has been appreciated. This breakthrough was due primarily to the discovery that some of these conductors could have appreciable conductivities - $\sim$0.5 ohm^{-1} cm^{-1} - at ambient temperatures. This advance has since been followed by considerable technological developments (1-3). The major interest has been directed to the development of efficient traction and energy-storage devices using secondary batteries and to the development of fuel cells. Other applications are also being developed, such as sensing devices in control systems, ion-specific electrodes and membranes, thermoelectric generators, and electronic circuit components, e.g., coulometers, bi-stable devices, reference voltage devices and electrochromic displays. Finally, it should be noted that solid electrolytes are an important research tool for thermodynamic and kinetic investigations.

Single crystal and dense polycrystalline Na β-Al_2O_3 and MgO- or Li_2O-stabilized Na β''-Al_2O_3 have been shown to be fast-ion conductors (4,5). The high conductivity of sodium in these materials is directly related to their crystal structures in which the sodium resides on a loosely packed plane. Major technological programs have already been initiated to use these two materials as electrolytes in secondary batteries, such as the sodium-sulphur battery. This is currently being actively developed in the U.S.A., United Kingdom, France, Germany and Japan for use in electric vehicles or for load levelling in power generation (6-8).

It is well established that the microstructures and hence the properties of ceramics depend strongly on the characteristics of the initial powder. In particular, the powders should be characterized by a high degree of homogeneity (chemical and physical) and high purity, while maintaining a very fine crystal size. A program was initiated at CANMET to study the preparation and fabrication of homogeneous powders. In this report the preparation of Na β-Al_2O_3 by the techniques of solution spray drying and spray freezing-freeze drying will be discussed with particular regard to the powder characteristics and their behaviour during calcination. An overview of the CANMET program is shown in Fig. 1.

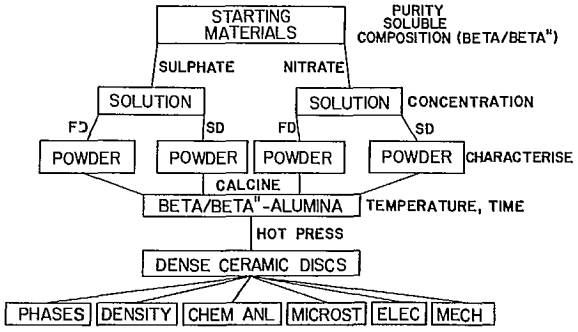

Fig. 1 - CANMET program on the preparation, fabrication and characterization of sodium beta- and beta"-alumina (Phase I)

LITERATURE SURVEY

The primary considerations for using solid state electrolytes in technical applications are the magnitudes of the ionic and electronic conductivities and the chemical stability in the cell environment. For example, the electrolyte in secondary batteries for vehicular propulsion must have a low resistivity to achieve the high power densities that are required. For the case of β''-Al_2O_3 in the Na-S battery a goal of 5 ohm-cm or less has been recommended (7). Such high power densities are not required for batteries being used in load-levelling but even so, a lower resistivity electrolyte would decrease the initial capital cost and also increase efficiency.

The ionic conductivities of single crystal Na β- and β''-Al_2O_3 are shown in Fig. 2 as a function of temperature (4). Included in this figure are the conductivities for the polycrystalline materials. It can be seen that β''-Al_2O_3 has the lower resistivity and hence is preferred for applications where high power densities are required. The polycrystalline resistivities are

somewhat lower than their respective single crystal values and this is probably due in part to the tortuosity of the conduction path. It has, however, also been shown that the resistivity-temperature relationship is also dependent on grain size (Fig. 3). This behaviour has been shown for β-Al_2O_3 to be a result of the intergranular resistance between grains and is therefore dependent on the nature of the grain boundary (9). Powers and Mitoff have also shown that the intergranular component is not only dependent on temperatures and composition but also on the microstructure (e.g., second phases) and other processing details (9). For example, they have shown that the milling procedure and the amount of porosity can greatly influence this intergranular component. A similar approach has also been taken by Virkar et al. (10) to evaluate the intergranular resistivity for Li_2O-stabilized β"-Al_2O_3. However, as pointed out by De Jonghe (11), it is difficult to make any quantitative correlations between grain boundary structure and these equivalent circuit approaches. It would appear from the above discussion that even when the correct composition has been chosen, it is still necessary to fabricate single-phase materials with large grain sizes, clean grain boundaries (high purity), high densities and reasonable homogeneity to achieve low resistivities. Clearly, some compromises may have to be made when other specifications have also to be met. For example, materials with large grain sizes would tend

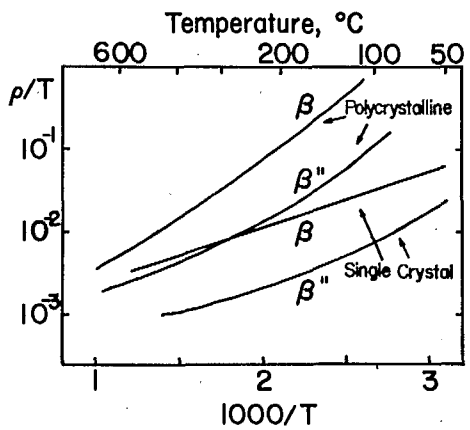

Fig. 2 - Variation of sodim ion conductivity with temperature (Ref. 9)

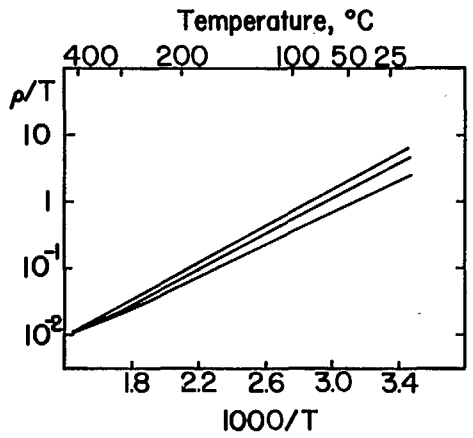

Fig. 3 - Variation of resistivity with temperature in three samples of polycrystalline beta-alumina of the same composition (9.5 wt % Na_2O and 0.25 wt % Li_2O) but of different grain sizes (After Ref. 63)

to give materials of low strength and hence could be unacceptable.

It has been shown that both β- and β"-Al_2O_3 can be fabricated with acceptable ionic and electronic conductivities for many applications, but problems have occurred in terms of durability, particularly in the Na-S battery. These problems are often related to the failure of the β- or β"-Al_2O_3 tube. Cell failure occurs as a result of fracture of the electrolyte or by short-circuiting when sodium penetrates the electrolyte. This electrolytic degradation has been shown to be associated with the formation and penetration of sodium either as grey filaments or as a general darkening extending from the sodium interface (12-16).

Several mechanisms have been put forward to explain this degradation. Initially, it was suggested that pre-existing cracks will propagate at high current densities as a result of the hydraulic pressure of the flowing sodium (17), this postulate has since been extended further to account for the effect of stress, capillarity and the selective removal of material from crack tips by the sodium (18,19). It is clear, however, that cells operating at relatively low current densities also fail and that other degradation mechanisms can play a role, e.g., discharge of Na^+

ions within the electrolyte can lead to local stresses (20), impurities present in the electrode can exchange ions with β- or β"-Al_2O_3 and produce stress gradients (21,22). As discussed before, it is clear that the degradation process will also be dependent on the microstructure of the electrolyte. For example, fabrication defects may act as sites for sodium penetration or formation. It has also been suggested by Powers and Mitoff (9) that their equivalent circuit model indicates that large electric fields are possible across grain boundaries or in the vicinity of large grains and this may play a role in the degradation process.

In addition to the above consideration, other specifications have also to be met for these solid-state electrolytes to be used in practical systems. These can include: reasonable strengths and thermal-shock resistance, to withstand stresses encountered during manufacturing, assembly and operation; high densities for hermeticity and to assure reasonable strengths; good wettability by the electrodes; and finally, close geometric tolerance for cell design. High strength ceramics are generally characterized by a small grain size and absence of cracks, pores, inclusions and internal stresses, as well as smooth surface finish. To meet these specifications, careful consideration must be given to the details of the ceramic fabrication process and in particular to the microstructure of the electrolyte.

The origin of the high conductivity in β- and β"-Al_2O_3 is directly related to their crystal structures, which are shown in Fig. 4. Both structures are layered and consist of blocks of four close-packed planes, which consist of oxygen and aluminum ions in a spinel-like structure. These blocks are separated by Al-O-Al columns. The sodium ions reside on the loosely-packed planes between the spinel blocks and can migrate readily in an electric field. The difference between the β- and β"-Al_2O_3 is essentially only in the stacking sequence of the close-packed layers.

The main features of the β-Al_2O_3 strucure were deduced by Bragg et al (23) and have been refined by other workers (24,25). The structure of β"-Al_2O_3 was originally determined by Yamaguchi (26) from X-ray powder diffraction data but as

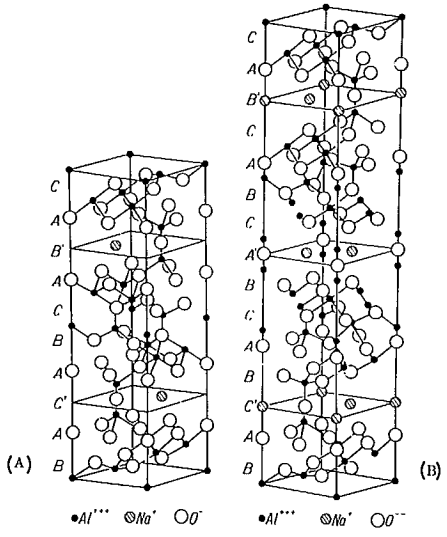

Fig. 4 - Crystal structures of (A) sodium beta-alumina and (B) sodium beta"-alumina (After Ref. 83)

this had been reported only in the Japanese literature, it was reported by Théry and Briancon (27) in 1962 as a new compound. The crystal structure was confirmed by Bettman and Peters (28) on a single crystal of MgO-stabilized β"-Al_2O_3. Powder diffraction patterns have also been reported by several other workers for β- and β"-Al_2O_3 (22,29-32). These patterns are often complicated by the epitaxial co-existence of both β- and β"-Al_2O_3 in the temperature range from about 1050 to 1550°C (32,33). Indeed, it has been observed that these phases can intergrow on a very fine scale (34,35) and can therefore complicate the X-ray diffraction intensities.

The phase diagram for the Na_2O-Al_2O_3 system has been proposed by Rolin (36) and critically reassessed by DeVries and Roth (37). In more recent times, the diagram has been further modified by Weber (38) (Fig. 5). In this diagram both β- and β"-Al_2O_3 are given as nonstoichiometric phases with narrow compositional limits. An alternative diagram has been put forward by Fally et. al (33) and is shown in Fig. 6. In this diagram the β-Al_2O_3 phase field is somewhat wider and at temperatures in the range of 1050 to 1550°C, the formation of β-Al_2O_3 is usually accompanied by the presence of the β" phase. Both diagrams indicate that β"-Al_2O_3 is metastable in the binary system.

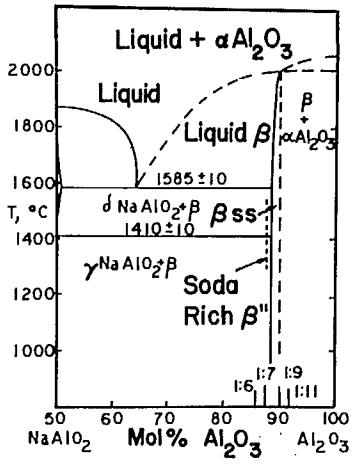

Fig. 5 - Section of Na_2O-Al_2O_3 pseudobinary phase diagram containing β and β"-alumina (After Ref. 38 and 84)

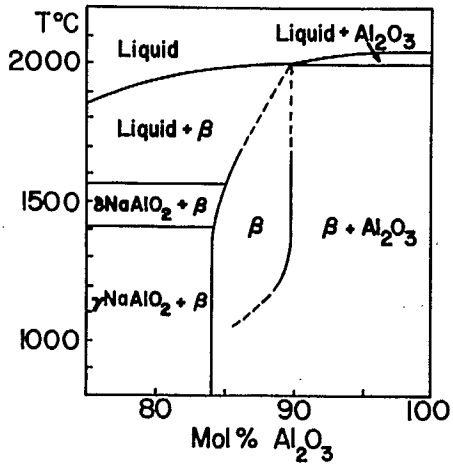

Fig. 6 - Phase equilibria in the Na_2O-Al_2O_3 pseudobinary system (After Fally et al., Ref. 33)

To stabilize the β" phase, dopants such as Li_2O and MgO are generally added to the system (39,40). These dopants will also increase the conductivity but, as pointed out by the Ford workers (41), the conversion to the β" phase is relatively slow so that after sintering the conversion to β" is incomplete. To overcome this problem the samples can be annealed after fabrication (41). It was also found that improving the distribution of Li_2O by adding $Li_2O.5Al_2O_3$ instead of Li_2CO_3 to the initial mix also led to a greater degree of conversion to β"-Al_2O_3 after both calcination and sintering (41). It is clear therefore that homogeneity in the lithium distribution is important for the conversion of β- to β"-Al_2O_3. To form β"-Al_2O_3 compositions of Li:Na:Al and Mg:Na:Al of approximately 0.16 to 0.25:1:5.0 to 6.3 are generally used. At lower soda levels, dopants have also been shown to lower the conductivity of β-Al_2O_3 (42,43).

Elliott and Huggins (44) have explored the $NaAlO_2$-Al_2O_3 phase diagram for temperatures between 800°C and 1150°C and have reported two new phases λ-$Na_2O.xAl_2O_3$ and a hydrated aluminate ρ-$Na_2O.Al_2O_3.6H_2O$.

The phase equilibria in these systems are also complicated by the high vapour pressure of Na_2O. For example, at 1527°C the vapour pressure is ∿0.02 mm of Hg. This tendency to lose Na_2O leads to the formation of α-Al_2O_3 at temperatures around 1500°C and even lower under reducing conditions (4). As sintering of both β- and β"-Al_2O_3 is carried out at temperatures above 1550°C precautions have to be taken to minimize or prevent soda loss. This has been accomplished by rapid firing (45), encapsulation in a covered or sealed vessel (41) or by surrounding the material by powder (46).

In the phase diagram, the presence of a eutectic at approximately 1585°C can give rise to a liquid phase during sintering depending on the choice of raw materials and the degree of mixing. It has been observed that higher soda concentrations result in higher sintering rates (47) and this may be a result of the presence of liquid phases accelerating the densification process. Indeed by choosing an additive with the eutectic composition, it has been shown that the densification of β-Al_2O_3 can be significantly improved(48).

As discussed earlier, to achieve the desirable properties of high conductivity, mechanical strength and durability, it is necessary to control the microstructure of the material. This control will depend on the details of the fabrication process. The fabrication of ceramics is usually accomplished in three principal steps: powder preparation, forming into the required shape and, finally, densification to remove pores and to develop other required properties. There is

invariably strong interaction between these steps.

Various powder preparation techniques have been attempted for β- and β"-Al_2O_3. These various powders can be classified according to their homogeneity, purity, crystal size, shape and degree of agglomeration. Often in ceramic fabrication use is made of liquid phase sintering to enhance densification rates, but for the β-aluminas the presence of a liquid phase may lead to the exaggerated grain growth that is often observed. As discussed earlier, the presence of this type of inhomogeneity will also tend to influence the final properties of the material, e.g., conductivity and durability. Similarly, the use of high purity raw materials would also be expected to give materials with superior properties. For solid state sintering, one generally expects that enhanced sintering rates can be accomplished using homogeneous powders with high surface areas, provided the powders are not highly agglomerated. For the β-alumina, enhanced sintering rates would be useful in reducing the problem of exaggerated grain growth and soda loss and, as pointed out earlier, it appears that homogeneity can also influence the conversion rate of β to β". Seeding techniques have also been used to control grain growth (49,50).

Two commercial powders of β-Al_2O_3 are available, but both are milled to reduce the grain size. Monofrax H (Carborundum) is obtained from a fusion process and Alcoa XB-2 is made by a Bayer process. Other workers have relied on the more traditional dry milling of the raw materials (e.g., Na_2CO_3 and α-Al_2O_3 (31,41). The milling of these materials will also tend to increase the impurity levels.

Clearly, a higher degree of homogeneity can be obtained if some or all of the raw materials are initially present as a liquid. For example, workers have also explored the techniques of solution spray drying (20,49), coprecipitation (20,49), gel processing (32,49,51) and stir drying (51) for producing β- or β"-Al_2O_3. In these techniques, it has been shown that the choice of raw materials can influence the phase formation and that the morphology of the powders can greatly influence the sinterability. For the β-aluminas the presence of needle-like or platey grains can lead to poor packing and hence to poor sintered densities (51). Similarly, even if the powders are of sub-micrometre size any agglomeration will lead to poor green structures (51). Powders often have to be modified after preparation to alter their forming characteristics e.g., de-agglomeration or spray drying.

Several different types of forming techniques have been used for polycrystalline β- and β"-Al_2O_3 and include extrusion (20,49), isostatic pressing (20,49), electrophoretic deposition (33, 52,53), slip casting (54,55) and centrifugal casting. Hot pressing, which is a technique that combines forming and sintering, has also been used (20,56-59). For the β-aluminas the major influence of the forming technique has been on the preferred orientation of the crystals. In a tubular configuration the orientation is such that the basal planes tend to line up parallel with the tube axis. In hot pressing the basal planes tend to lie perpendicular to the hot pressing direction. This preferred orientation will lead to anisotropy in the sodium ion conduction. For hot-pressed (56,59,60), isostatic pressed and sintered (60,61), and extruded materials (20) the ratio of the ionic conductivities parallel and perpendicular to the texture axis seems to be generally less than 2 to 3. For slip casting, however, a ratio of 40 has been measured (54).

β- and β"-Al_2O_3 are generally sintered using either a batch technique or a zone sintering technique (45). Atmosphere control is important in the sintering of the β-aluminas because of the soda loss problem discussed earlier. It has also been shown that higher densities can be obtained when the materials are sintered in oxygen (62) and that careful control of the temperature must be maintained to reduce the problem of exaggerated grain growth (63).

The initial emphasis of the program at CANMET has been on the preparation of β- and β"-Al_2O_3 powders. Two techniques - solution spray freezing-freeze drying and solution spray drying - were chosen, as these generally produce high purity, homogeneous, reactive powders. (As pointed out in this discussion, these characteristics

should aid in the fabrication of the β-aluminas, particularly in the formation of uniform, fine-grained microstructures and should result in materials with superior properties.) Both techniques use a solution of the required ions as a starting point and the solvent is removed in such a way as to retain, as much as possible, the homogeneity of the original solution.

FREEZE DRYING

The freeze drying method (64) consists of rapidly freezing a solution containing the required cations. The solid is then freeze-dried to remove the solvent. The aim of the process is to retain the homogeneity of the solution by rapid freezing and then to remove the solvent without the formation of any liquids. After freeze drying, the product must be heat treated to decompose the salts and the salts should be selected so that there is no melting or volatilization during this treatment. After decomposition the salts are usually ultrafine which enhances reactivity and also precludes the need for any milling procedures which could otherwise lead to contamination of the material. The powders are, however, usually agglomerated after drying and calcining so that it is often necessary to de-agglomerate by some powder modification technique. It is useful at this point to describe some of the details of the freeze drying process.

Water is frequently chosen as the solvent and soluble salts such as sulphates, nitrates, oxalates, etc., are chosen as the raw materials. The solution is rapidly frozen usually as a spray into a cryogenic liquid, e.g., liquid nitrogen. It is clearly important to establish the freezing conditions so that phase separation does not occur. For example, consider the phase diagram for the $Al_2(SO_4)_3$-H_2O system, Fig. 7, which can be formulated from solubility data. For the cooling of the solution, marked A, the equilibrium process would be the formation of ice as the temperature falls below the liquidus curve until at the eutectic temperature the remaining liquid solidifies into ice and $Al_2(SO_4)_3.16H_2O$. For more rapid freezing, the degree of phase separation would be expected to decrease and at higher freezing rates

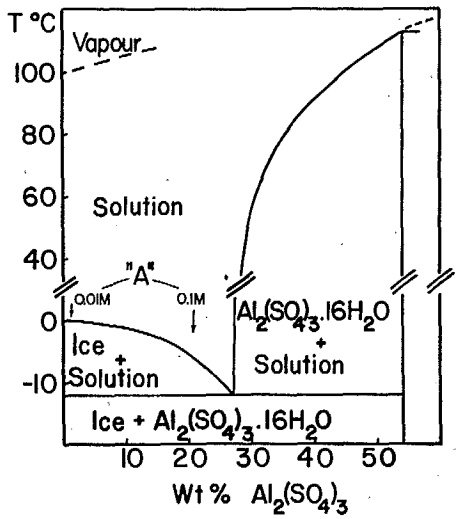

Fig. 7 - Phase equilibria in the $Al_2(SO_4)_3$-H_2O pseudobinary system

the crystallization of one or both phases may be suppressed completely. The freezing process does not appear to have been studied in great detail, but it has been shown from thermal analysis that the rapid freezing of $Al_2(SO_4)_3$ solution in liquid nitrogen at cooling rates between 15°C and 170°C per minute does give an amorphous phase (65). The inhibition of crystallization is expected to depend on the chemical nature of the solution and its tendency to form glass-like material. The rapid cooling of $MgSO_4$ at a rate of 15°C per minute indicated that crystallization did occur. It has, however, also been suggested that phase separation should be allowed to occur to some degree, otherwise there will be a tendency for the glassy phase to melt during drying at a temperature well below the eutectic temperature (66). Indeed, it has been suggested that NH_4OH should be added to the solution to increase the freezing point and to enhance phase separation (66).

After freezing, the mixture must be placed in a freeze drier to sublime the ice. A schematic representation of a freeze drier is given in Fig. 8. It consists of a chamber that can be evacuated to a pressure below the cryohydric point so that the ice sublimes directly into vapour. A temperature-pressure phase diagram for a salt-water system is shown in Fig. 9, where Q is the cryohydric point. Clearly the lower pressure

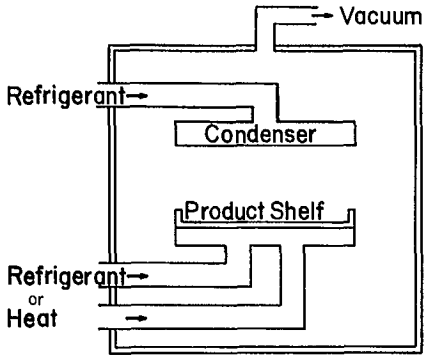

Fig. 8 - Schematic diagram of a commercial freeze drier

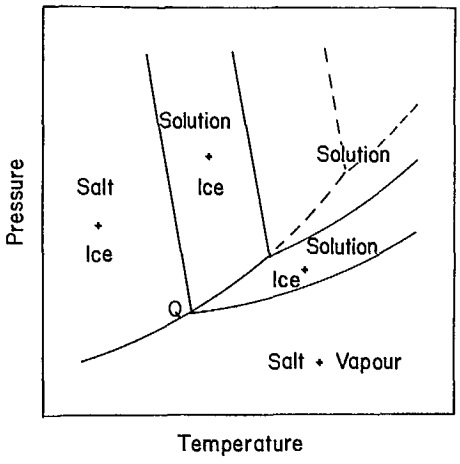

Fig. 9 - Phase equilibria in a salt-water system. Dotted line refers to pure water and solid line to salt-water mixture

changes the phase relations in Fig. 7 but, in general, the effect of pressure on the solubility curve is expected to be relatively small except that the equilibrium is now between vapour and solid. It is also important to maintain the temperature of the frozen solid below the eutectic temperature until the pressure is below Q, otherwise melting can occur. During freeze drying, the water vapour is condensed on a cold surface and hence effectively removed from the system. The temperature of the condenser is maintained well below that of the frozen product usually at between -40° and -60°C as the sublimation rate will depend on the difference in temperature between the product and the condenser. The sublimation rate will also depend on the pressure within the system. In a freeze drier, heat can be supplied to the frozen product to control its rate of drying. Because a dynamic equilibrium is established during freeze drying, the vapour pressure in the powder can rise above Q if too much heat is supplied and "melt back" can occur. To prevent this, the thermal energy supplied to the product must be carefully controlled. Alternatively, the temperature can be maintained below the eutectic or melting temperature throughout the drying process.

For the β-aluminas, information on the phase equilibria for the aluminum salt-sodium salt-water system would be useful to determine the eutectic temperature. To the authors' knowledge, only the $Al_2(SO_4)_3$-Na_2SO_4-H_2O system has been studied (67). The phase diagram for this system is shown in Fig. 10, and the ternary eutectic temperature is given as -10°C.

After the removal of ice, further dehydration can be carried out to remove any bound water, e.g., water of crystallization. This can usually be performed at higher temperatures (up to 100°C in commercial freeze driers) as there are no liquid phases in the system. A typical drying cycle is shown in Fig. 11.

As the freeze-drying process should be performed in the solid state, the homogeneity of the original solution is expected to be retained to a high degree. Although X-ray mapping tech-

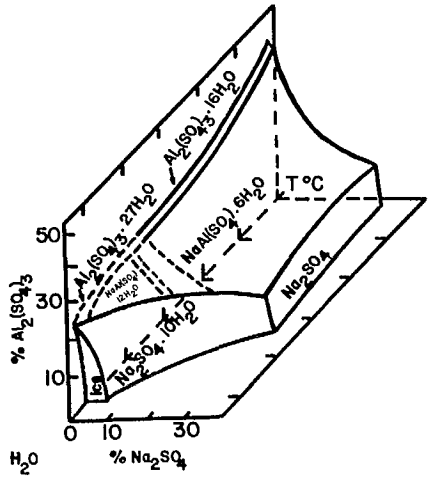

Fig. 10 - Phase equilibria in the ternary system $Al_2(SO_4)_3$ - Na_2SO_4 - H_2O (After Ref. 82)

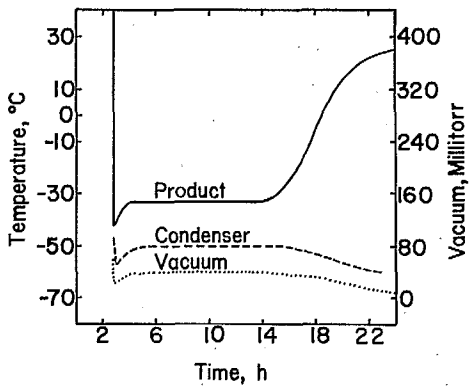

Fig. 11 - Typical conditions in a freeze drier during the sublimation (drying) stage

niques have been made to substantiate this assumption, it has also been shown that the conductivity of freeze-dried Cd-doped AgCl is high and that the optical homogeneity of lanthanum-doped lead zirconate titanate (PLZT) is good (68) thus indicating that the powder homogeneity was very good-(69). It is also generally found that the decomposition and formation of the final product occurs at lower temperatures than for powders prepared by other techniques (65). However, heterogeneity may develop during calcination and sintering of freeze-dried powders as a result of, for example, rehydration and melting, sublimation, liquid phase formation, second phase formation or redox processes.

Finally, the morphology of the freeze-dried powders is also of importance as this will determine the green structure of powder compacts. It has been shown that the spherical morphology of the frozen spheres is retained during drying and calcining but that the spheres consist of radial chained aggregates of crystallites (70). It was also shown that grain growth exponents are low for freeze-dried powders and that this inhibition of grain growth probably results from the high porosity of the spherical agglomerates (70).

The technique of solution spray freezing-freeze drying has been attempted for several mixed oxides and these include $MgAl_2O_4$, lithiated NiO, $NiCo_2O_4$ (71), PLZT (68), and doped $LaMnO_3$ (72). Freeze drying has also been reported recently for β-Al_2O_3 (51), though it was indicated that the powders had poor sinterability. From this discussion, it would appear that solution spray freezing-freeze drying is a simple and noncontaminating powder preparation technique in which compositions can be formulated from high purity reagents with minimal contamination. The powders can have a high degree of homogeneity and therefore offer the opportunity of producing fine-grained, uniform ceramic microstructures.

SPRAY DRYING

In the technique of solution spray drying, a solution containing the required cations is sprayed into a heated chamber, as shown schematically in Fig. 12. Depending on the temperature of the chamber, the solvent will be removed and decomposition can occur. As this process should occur rapidly, the resultant powders would be expected to be homogeneous and fine grained. This technique has been used to produce mixed oxide powders of $CaAl_2O_4$ (73), PLZT (68), $MgAl_2O_4$ (74) and several different ferrites (74-76). It is also a process that promises ease of scaling-up (77). The powders are usually amorphous or poorly crystalline after drying and in the case of $NiFe_2O_4$ were shown to form the spinel and sinter at lower temperature than normal, again an indication of good homogeneity. In comparison with the freeze-drying technique, it has been shown that

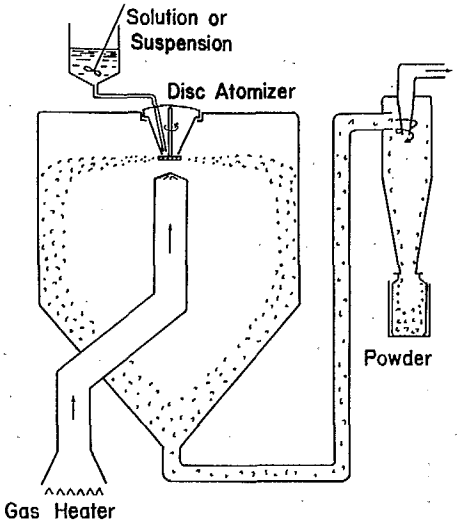

Fig. 12 - Schematic of a commercial spray drier

spray drying introduces a greater contamination but that the reactivities were similar (78). In that work it was noted that the major influence on powder characteristics was the choice of raw materials, e.g., nitrates or sulphates, etc.

There appears to be few studies on the structure of spray-dried powders though it was indicated by de Lau (74) for spray-dried sulphates that the powder was in the form of hollow spheres after drying. After calcining, the hollow spheres were aggregates of very fine crystals, but these could be easily broken down in a turbine mixer before pressing and sintering. It was also noted that the properties of ferrites were improved by using spray-dried powder.

In this study the two powder-preparation techniques were used for the formation of β-or β"-Al_2O_3. In particular, an attempt was made to understand the powder characteristics and the processes that occur during the drying and calcining stages.

EXPERIMENTAL PROCEDURE

SOLUTION SPRAY FREEZING-FREEZE DRYING

A solution was made up of high purity Na_2CO_3 and $Al_2(SO_4)_3.16H_2O$ dissolved in distilled water at room temperature. The two starting materials had previously been checked for their weight loss so that the solution would produce powder with the composition $Na_2O.6Al_2O_3$ after drying and decomposition. The concentration of the solution was 0.02 M with respect to the Na_2CO_3. This solution would be expected to yield approximately 15 g/L of calcined $Na_2O.6Al_2O_3$. It was noted that a gas, presumably CO_2, was evolved during solution preparation when the Na_2CO_3 was added to the acidic sulphate solution.

The starting solution was rapidly frozen by spraying into liquid nitrogen using a pneumatic jet (79). The frozen mixture was then freeze dried in a commercial drier. Initially the shelf temperature was controlled at -15°C to reduce the possibility of melting. After the powder was relatively dry, the shelf temperature was raised to 28°C for final drying. A short study was also made to determine whether changing the concentration of the starting solution, the freezing-rate, drying temperature or the identity of the sodium anion altered the powder characteristics.

An attempt was also made to produce powders based on solutions of $NaNO_3$ and $Al(NO_3)_3$ but it was found that these materials tended to melt during freeze drying. It has been suggested previously that this difficulty in freeze drying $Al(NO_3)_3$ is a result of its low freezing point and its tendency to form a glass during freezing (66).

SOLUTION SPRAY DRYING

A solution of Na_2CO_3 and $Al_2(SO_4)_3.16H_2O$ was prepared in a similar fashion to that described above. In this case, however, the solution was saturated with respect to the two components at ∿0.25M. The solution was split into two lots, one being freeze dried as described previously and the other being spray dried in a commercial spray drier. For the latter process, the solution was dried using an inlet temperature of 360° to 400°C and an outlet temperature of 120°C. The solution feed-rate was approximately 7 L/h. A saturated solution was also prepared using $NaNO_3$ and $Al(NO_3)_3.9H_2O$ which was then spray dried using the same conditions.

POWDER CHARACTERIZATION

After drying, it was necessary to calcine the spray-dried (SD) and freeze-dried (FD) powders to decompose the salts and to produce β-Al_2O_3. The calcination process was studied using a variety of techniques. Thermogravimetric analysis (TGA) was carried out on the dried powders in air using a thermobalance and a heating rate of 12°C/min. Differential thermal analysis was carried out on the powders using the same heating rate as in the TGA. The powders were calcined in air for a period of 1 h at a series of temperatures up to 1400°C. The samples were then analyzed by X-ray diffraction using Guinier focussing and Debye-Scherrer cameras, and CoK_α radiation) to identify the phases present, by nitrogen adsorption to determine the specific surface areas, and by chemical methods to determine the Na, Al and S concentrations. A series of samples was also calcined at 1300°C for different periods of time and

then analyzed in a similar fashion. The purity of the calcined powder was determined by emission spectrography. A few samples were also analyzed using infrared absorption spectroscopy.

Finally, the physical characteristics of the powders, before and after calcination, were studied using optical, scanning electron (SEM) and transmission electron microscopy (TEM).

RESULTS AND DISCUSSION

FREEZE-DRIED $Na_2O.6Al_2O_3$

After drying, the FD powder was observed in the optical and scanning electron microscopes. In the optical micrograph of Fig. 13, it can be seen that the powder is in the form of spheres, which is a result of the spray freezing process. The average size of the spheres was determined to be 120 μm. For pneumatic jets, the average droplet size depends on several parameters (80). For a particular liquid and jet, however, the average droplet size will simply depend on the relative velocity of the atomizing gas with respect to that of the liquid so that the average droplet size decreases for an increasing gas velocity. For example, it was found that the average size of the FD spheres could be decreased by a factor of two to three with the equipment used in this work.

When observed in the SEM, the spheres are seen to be porous and permeated with fine channels ~0.5 μm in diameter, as shown in Fig. 14 and 15. It is presumably from these channels that the ice has been sublimed during freeze drying.

After drying, the powders were amorphous to X-ray diffraction but it is not clear whether the non-crystallinity is due to the rapid freezing process or to the dehydration of the $Al_2(SO_4)_3.16H_2O$ in the vacuum during drying. In terms of powder homogeneity it is clearly important to know whether phase separation occurs or not during processing and if so, to what extent. This point will be discussed later but it was noted that the FD powders absorbed water quite readily from the atmosphere. In Fig. 16, a comparison is shown of the X-ray patterns for the as-dried powder immediately after drying and after four months storage. Several lines have appeared in the X-ray pattern and these were sufficient to identify $Al_2(SO_4)_3.16H_2O$.

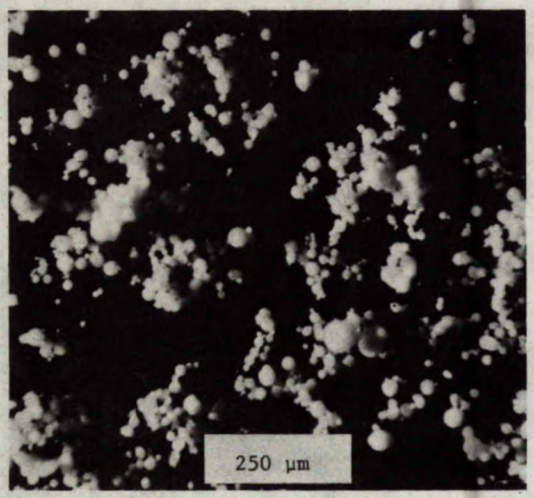

Fig. 13 - Optical micrograph of freeze-dried powder

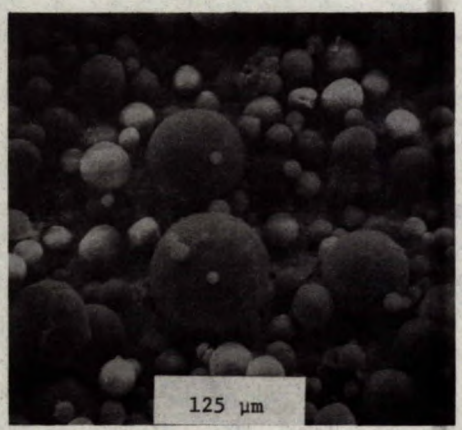

Fig. 14 - Scanning electron micrograph of freeze-dried powder

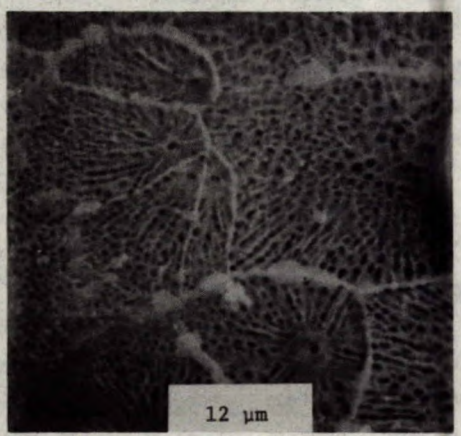

Fig. 15 - Surface of freeze-dried sphere

The infrared spectrum of the dried powder is given in Fig. 17 and has 4 major peaks at 3200, 1650, 1130 and 600 cm^{-1}. The spectrum of the FD powder is very similar to that of $Al_2(SO_4)_3.18H_2O$ except that peaks are absent at 950 and 620 cm^{-1}. The first two peaks observed for the FD powders are typical O-H stretching and H-O-H bending modes for absorbed water. The other two peaks are the two normal modes of vibration that are infrared active for the SO_4^{2-} ion. The absence of the peaks at 950 and 620 cm^{-1} is indicative that the SO_4^{2-} ion is not distorted (81).

The results of the X-ray diffraction analysis on the calcined powders are summarized in Table 1. By 400°C the amorphous, as-dried powders have crystallized into $Al_2(SO_4)_3$. Several other lines were observed in this pattern but these could not be positively identified. Presumably the other phase contains the sodium. Above 800°C the $Al_2(SO_4)_3$ decomposes and Na_2SO_4 is also formed, which is stable to about 1200°C. The Na_2SO_4 decomposes at this temperature and reacts with the η-Al_2O_3 to form β"-Al_2O_3. Part of the X-ray spectrum is shown in Fig. 18 for a sample calcined at 1250°C for 1 h. The asymmetry of the 19.7 nm (1.97 Å) β"-Al_2O_3 peak at No. 10 indicates that some β-Al_2O_3 is probably also present in the powder as it has been shown that these two phases tend to intergrow on a fine scale (3,4). At higher temperatures of 1300°C to 1600°C or for longer times, the presence of both phases is readily apparent. Above 1550°C, the amount of β-Al_2O_3 decreases more rapidly but is still observed at 1650°C after 1 h. This behaviour is in agreement with the phase diagram of Fally et al. (Fig. 6) where the β"-Al_2O_3, is considered to be metastable. The phase transformation of β"- to β-Al_2O_3 is rather sluggish. The powder pattern for the FD powder calcined at 1250°C that produced the best crystallized sample of β"-Al_2O_3 was indexed and the relative intensities were measured using both Debye-Scherrer and Guinier cameras. The re-

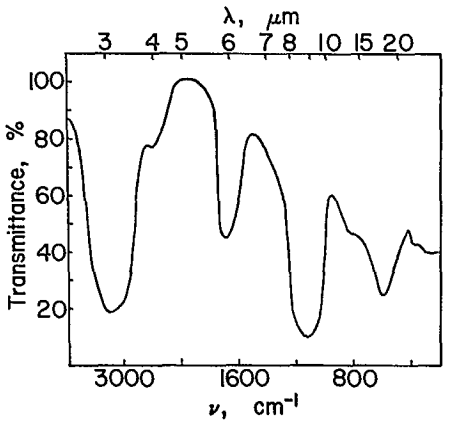

Fig. 17 - Ir spectrum of as-prepared powder obtained by freeze-drying a 1:6 sulphate solution

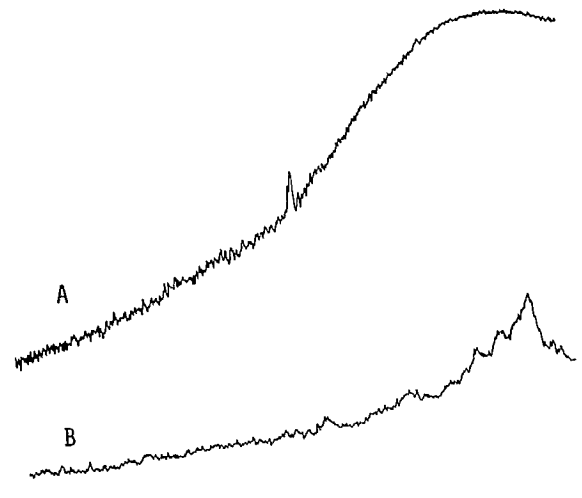

Fig. 16 - X-ray diffraction pattern a) immediately after drying b) 4 months after drying

Table 1 - Phase sequence for freeze-dried powder

Temperature (°C)	Phases
As dried	Amorphous
200	
400	$Al_2(SO_4)_3$ + ?
600	
900	η-Al_2O_3 + Na_2SO_4
1000	
1100	
1200	η-Al_2O_3 + Na_2SO_4 + β"-Al_2O_3
1250	β"-Al_2O_3
1300	
1400	β"-Al_2O_3 + β-Al_2O_3
1500	
1600	

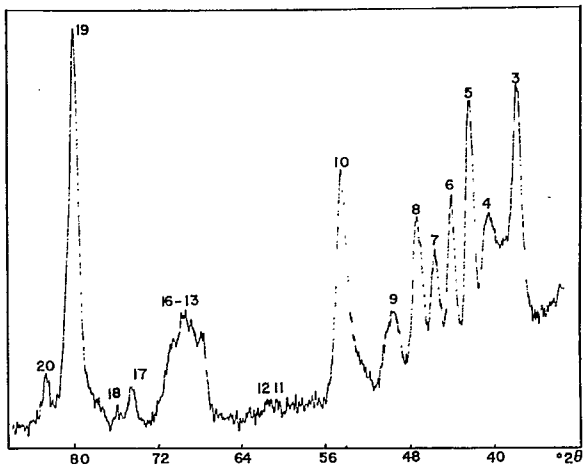

Fig. 18 - Debye-Scherrer X-ray diffraction pattern for Na β"-Al_2O_3 (CoK_α radiation, Fe filter)

sults are given in Tables 2 and 3. The calculated lattice parameters are compared with previous literature data in Table 4. The powder pattern calculated from a single crystal study of MgO-doped β"-Al_2O_3 is given in Appendix A.

The presence of a large amount of β"-Al_2O_3 in the calcined powder was unexpected when compared with other work in the literature. As shown in Fig. 19, this effect could be related to the similarity between the η-Al_2O_3 and β"-Al_2O_3 structures.

It is clear from these results that the chemical reactions during calcination are very important. Instead of retaining the high degree of homogeneity expected for FD powders, two distinct phases are formed, i.e., η-Al_2O_3 and Na_2SO_4. The latter does not decompose until temperatures above 1200°C and is, moreover, present as a liquid. The melting point of Na_2SO_4 is approximately 890°C. It is possible that other liquids may be formed during calcination. For example, sulphates including $Al_2(SO_4)_3.16H_2O$ tend to "melt" in their own water of crystallization and liquid phases are present in the Na_2SO_4-$Al_2(SO_4)_3$ system (6). The presence of such liquids would be expected to cause powder agglomeration, an effect that was observed. It was found that the powders readily break down under low pressures into ultrafine crystals.

On heating to 1000°C, the FD powder undergoes a 71% weight loss which occurs in two stages as shown in Fig. 20. The first stage is dehydration and for the FD powder it represented the loss of 7 mol of water per mole of $Al_2(SO_4)_3$.

Table 2 - X-ray diffraction pattern sodium beta"-alumina (Debye-Scherrer)

Peak	d(Å) observed	hkl	d^c(Å) calculated	I/Io
1	11.1	003	11.3	100
2	5.72	006	5.65	45
3	4.64	012	4.67	5
4	2.806	$00\bar{1}2/110/10\bar{1}0$	2.825/2.804/2.780	40
5	2.617	$01\bar{1}1$	2.602	20
6	2.514	116	2.512	30
7	2.415	021	2.420	25
8	2.334	024	2.344	20
9	2.251	119	2.249	25
10	2.146	$027/01\bar{1}4$	2.171/2.167	10
11	1.975	$02\bar{1}0$	1.974	40
12	1.820	122	1.826	VF
13	1.766	$02\bar{1}3$	1.777	VF
14	1.615	$00\bar{2}1$	1.614	15
15	1.599	$02\bar{1}6$	1.596	15
16	1.575	$12\bar{1}1$	1.577	15
17	1.549	$036/20\bar{1}7$	1.556/1.541	15
18	1.484	$02\bar{1}9$	1.487	VF
19	1.437	039	1.438	5
20	1.402	220	1.401	60
21	1.391	$20\bar{2}0$	1.390	VF
22	1.360	226	1.360	5
23	1.299	$02\bar{2}2$	1.301	5
24	1.210	402/042	1.213/1.211	10
25	1.199	404	1.201	5
26	1.175	$31\bar{1}4/10\bar{2}8$	1.176/1.175	5
27	1.134	$00\bar{3}0$	1.130	20
28	1.058	$22\bar{2}1$	1.058	25
29	1.050	$40\bar{1}6$	1.053	20
30	1.039	$04\bar{1}7$	1.037	20
31	1.019	419	1.020	15
32	.9871	$04\bar{2}0$	.9871	20
33	.9417	$00\bar{3}6$	.9417	15
34	.9352	$22\bar{2}7$	.9350	20
35	.9280	$03\bar{3}0/50\bar{1}1$	.9265/.9258	25
36	.9211	336	.9215	25
37	.9170	241	.9168	20
38	.9119	244	.9118	15
39	.9070	339	.9065	20

d^c - Calculated lattice spacing using lattice constants from Table 4

It was subsequently found that the amount of water lost was dependent on the drying conditions, e.g., shelf temperature and vacuum, and also on the time and method of storage. The second stage, which occurs between 700 and 900°C, is due to the decomposition of $Al_2(SO_4)_3$. The weight loss in this stage is equivalent to the loss of 17 mol of SO_3 per 6 mol of $Al_2(SO_4)_3$. The other mol of SO_3 is used in the chemical reaction to form Na_2SO_4. It is clear that at higher temperatures other weight losses will occur due to the decomposition of Na_2SO_4 and the loss of Na_2O from β- or β"-Al_2O_3. The DTA trace for the FD powder is given in Fig. 21 and shows three peaks. These peaks correlate with the loss of water at 180°C, the crystallization (xaln) of $Al_2(SO_4)_3$ at 500°C and the decomposition of $Al_2(SO_4)_3$ at 800°C.

The formation of β"-Al_2O_3 at approximately 1250°C is associated with a large decrease in specific surface area (Fig. 22), which is equivalent to an increase in equivalent spherical diameters from 35 to 24.5 nm (350 to 2400 Å). The specific surface area at 1250°C is still above

Table 3 - X-ray diffraction pattern for sodium beta"-alumina (Guinier)

Peak	d(Å)	I/Io	hkl	d^c(Å)
1	11.2	100	003	11.3
2	5.65	45	006	5.65
3	4.65	5	012	4.67
4	4.20	5	014	4.21
5	2.812	10	$110/00\bar{1}2$	2.804/2.825
6	2.792	50	$01\bar{1}0$	2.780
7	2.600	15	$01\bar{1}1$	2.602
8	2.500	60	116	2.512
9	2.413	40	021	2.420
10	2.327	25	024	2.334
11	2.275	10	025	2.285
12	2.256	10	$00\bar{1}5$	2.260
13	2.245	30	119	2.249
14	2.158	10	$01\bar{1}4$	2.167
15	1.968	35	$02\bar{1}0$	1.974
16	1.612	10	$11\bar{2}1/21\bar{1}0$	1.614/1.613
17	1.590	10	$02\bar{1}6$	1.596
18	1.574	10	$12\bar{1}1$	1.577
19	1.561	10	$11\bar{1}8$	1.563
20	1.549	10	$20\bar{1}7/036$	1.541/1.556
21	1.482	10	039	1.487

d^c - Calculated lattice spacing using lattice constants from Table 4

Table 4 - Lattice parameters for sodium beta"-alumina (without stabilizer)

a(Å)	c(Å)	Source
5.61	33.9	This work
5.597	33.95	Dyson and Johnson
5.60	34.11	Ray and Subbarao
5.61	33.95	Théry and Briançon

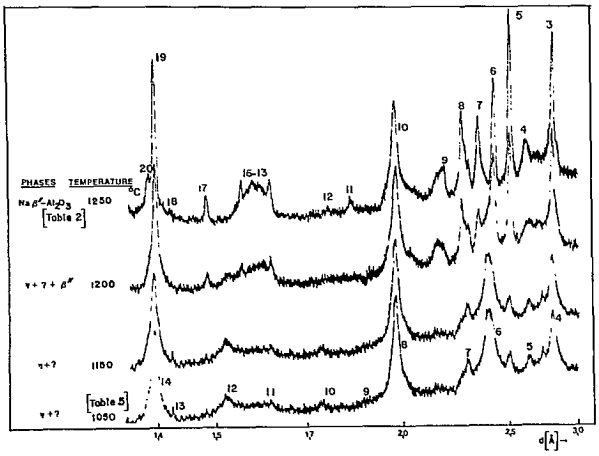

Fig. 19 - Guinier X-ray diffraction patterns for calcined phases

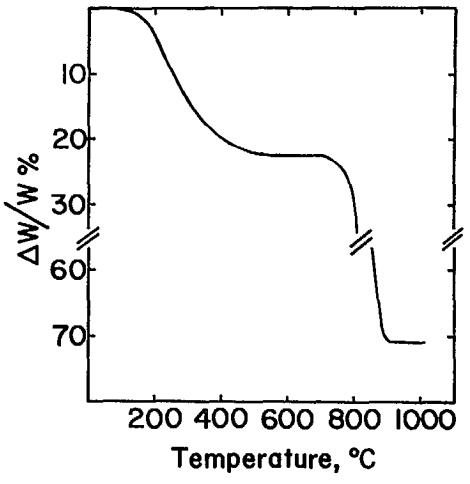

Fig. 20 - TGA for freeze-dried powder

15 m^2/g and, as shown by Johnson and Schnettler (70), the porous nature of freeze-dried $Al_2(SO_4)_3$ powders tends to limit crystal growth and hence they retain a high specific area. For example, the volume fraction of porosity in the FD β"-Al_2O_3 powder in this study is approximately 0.99.

It is well known that the Na β-aluminas are prone to soda loss at high temperatures. For the high surface area FD powder, it would be expected that such losses could be significant. In Table 5, the results of the chemical analysis for samples calcined between 1000 and 1400°C are presented. It can be seen that up to 1200°C the Na_2O content increases due to the decomposition of Na_2SO_4. At higher temperatures, however, the soda content decreases and is indicative of volatilization of the Na_2O from the β"-Al_2O_3.

Microscopic observations were made on the powders calcined at 1250°C for 1 h. In the scanning electron micrographs of Fig. 23 and 24 it can be seen that the powders still consist of porous spheres some of which have agglomerated with each other. The volume fraction and size of the porosity has clearly increased from that initially observed on the as-dried powder. The FD spheres at this stage must be complex aggregates of the submicrometre β"-Al_2O_3 crystals. In an attempt to identify the nature of the aggregation and the size and morphology of the crystals, a sample of the calcined powder was dispersed on a carbon film for observations in a TEM. As can be seen in Fig. 25, even after dispersion the powder is still highly agglomerated. Figures 26 and 27 are dark- and bright-field micrographs at a higher magnification. The diffracting crystals in the dark field micrograph (white) appear to be approximately 10.0 nm (1000 Å) in diameter. Finally, the electron micrographs of Fig. 28 and 29 show the presence of a highly faulted crystal. It was observed that the individual crystals had no definite morphology but were thin having a high transparency to an electron beam, and were often strained.

For the spray freezing-freeze drying process, it is important to ascertain the influence of the process parameters on the powder characteristics. For a solution of a particular composi-

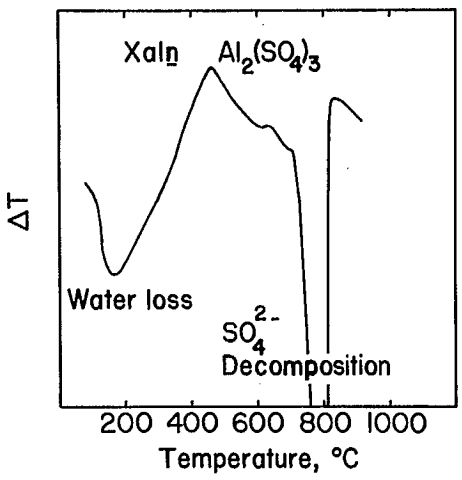

Fig. 21 - DTA trace for freeze-dried powder

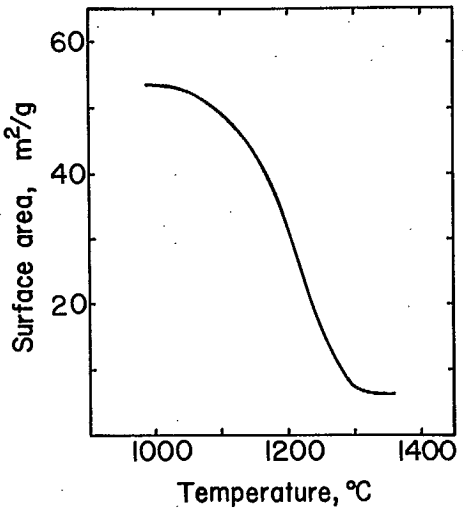

Fig. 22 - Specific surface area of freeze-dried powder calcined in air for 1 h at the temperatures indicated

Table 5 - Chemical analysis of freeze-dried powder

Temperature (°C)	Na_2O (wt %)	Al_2O_3 (wt %)	Al/Na (moles)
1000	7.63	82.3	6.6
1100	7.76	83.8	6.6
1200	8.07	89.8	6.7
1300	7.82	92.4	7.2
1400	7.63	93.9	7.5

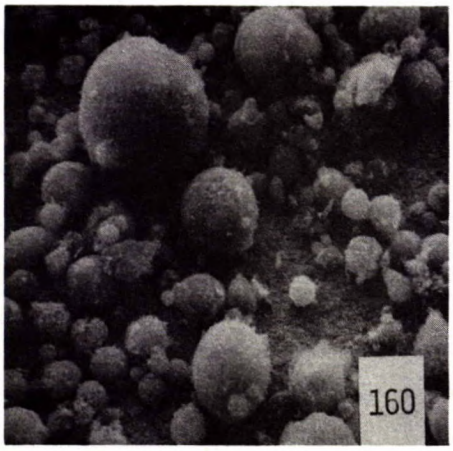

Fig. 23 - Scanning electron micrograph of calcined freeze-dried powder (1250°C, 1 h)

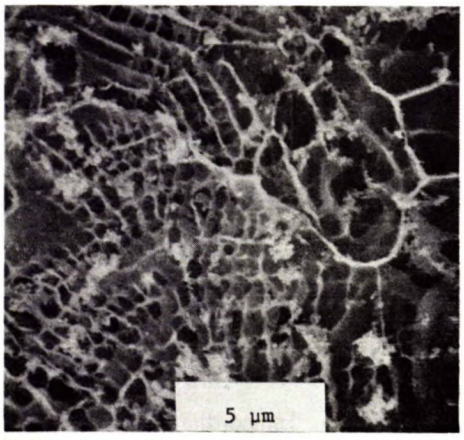

Fig. 24 - Surface of calcined, freeze-dried sphere (1250°C, 1 h)

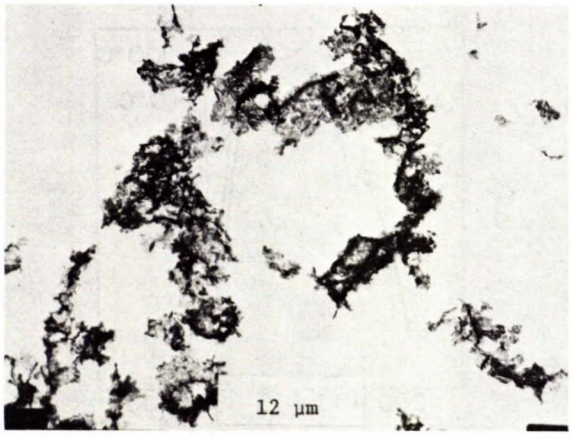

Fig. 25 - Electron micrograph of calcined freeze-dried powder

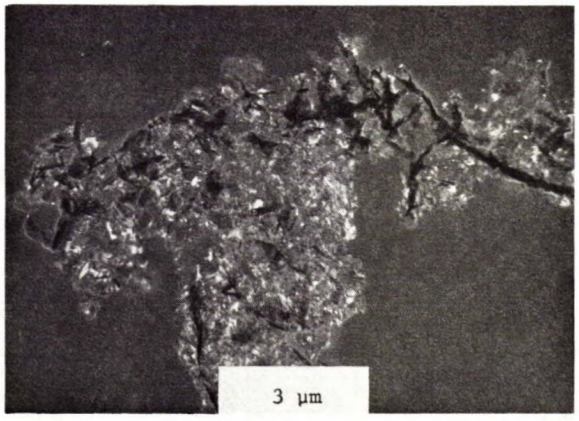

Fig. 26 - Electron micrograph of calcined freeze-dried powder (1250°C, 1 h) viewed in dark field

Fig. 27 - Electron micrograph of calcined freeze-dried powder (1250°C, 1 h) viewed in bright field

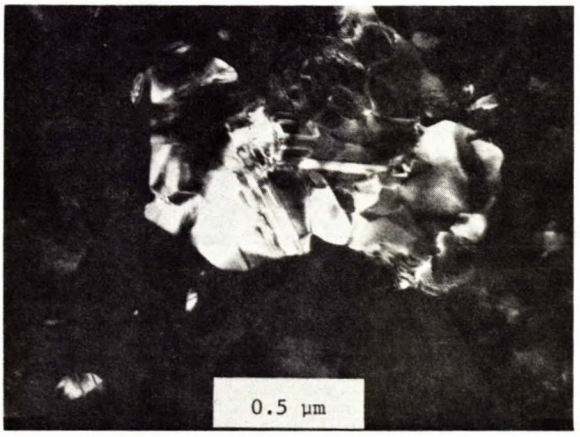

Fig. 28 - Dark field electron micrograph

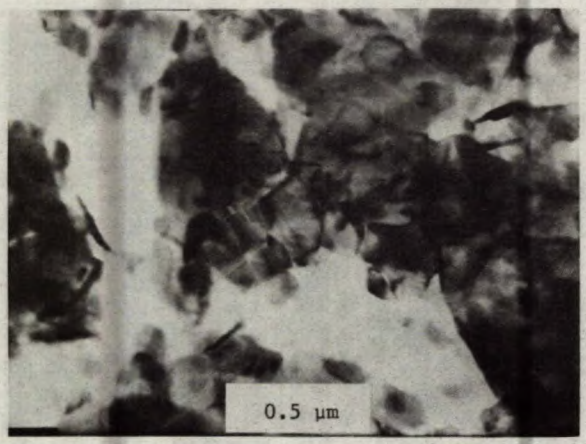

Fig. 29 - Bright field electron micrograph

tion and concentration it would be expected that the major variable during freezing would be the freezing rate i.e. droplet size and the quenching temperature difference whereas in drying, the major variables would be the temperature difference between the sample and the condenser, the system pressure, the shelf temperature and the drying time. A brief study of some of these variables, that is, shelf temperature and freezing rate, indicated that they did not lead to any substantial changes in the phase sequence, specific surface areas or chemical analysis. The major influence of the shelf temperature appeared to be in the nature and content of the water remaining in the powder after drying. Figure 30 shows the TGA curves for samples dried with different shelf temperatures. Clearly, a higher shelf temperature gives rise to a lower water content and also a more gradual loss of water during calcination. This behaviour is also reflected in the DTA traces for such powders (Fig. 31), where the water-loss peaks change their character. It is important to note here that comparison of water-loss rates or water contents should only be done for powders dried under the same conditions or for powders with equivalent water contents.

Some effort was also made to assess the effect of changes in the chemistry of the starting solution. For example, because the powders are decomposed after drying, any soluble sodium or aluminum salt could be chosen as a starting material. There are only two aluminum salts with high solubilities: $Al_2(SO_4)_3$ and $Al(NO_3)_3$. Attempts to freeze-dry solutions based on $Al(NO_3)_3$ proved unsuccessful because the frozen powders invariably melted during drying. Solutions, however, were made using a variety of sodium salts. The anions used were citrate, nitrate, hydroxide, acetate and sulphate. It was found again that the choice of sodium salt did not lead to any major changes in the power characteristics. There were, of course, slight variations in the TGA and DTA data due to the different decomposition temperatures of the salts but even so the powders all formed η-Al_2O_3 and Na_2SO_4 once the $Al_2(SO_4)_3$ de-

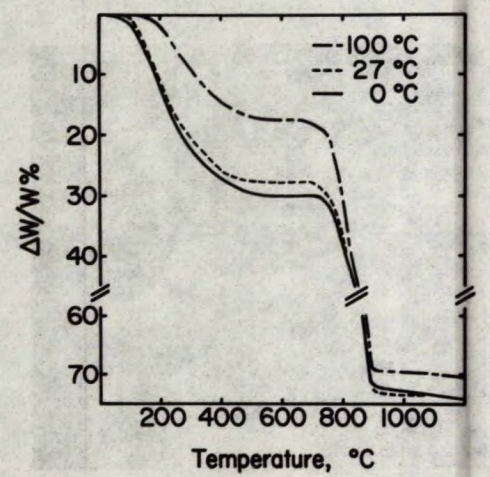

Fig. 30 - TGA of as-prepared powder after freeze drying at different shelf temperatures

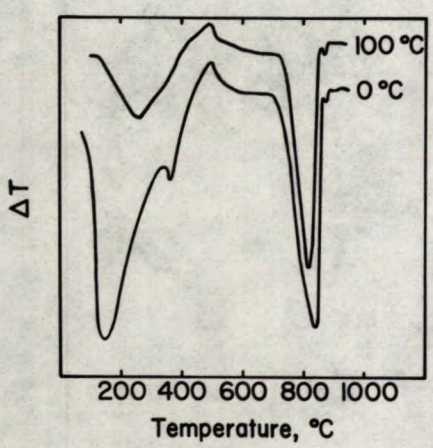

Fig. 31 - DTA of as-prepared powder after freeze drying to the shelf temperatures indicated

composed at approximately 840°C. Therefore, once calcined above this temperature, the powders had very similar characteristics.

Finally, the effect of variations in the concentrations of the starting solution was also studied. The starting materials were $Al_2(SO_4)_3 .16H_2O$ and Na_2CO_3, the concentrations were 0.01 M and 0.05 M with respect to the Na_2CO_3 and both powders were freeze dried under the same conditions. The solution concentration could influence the freeze-drying process by changing the freezing point of the solution and could influence the powder characteristics by changing the ice:salt ratio in the frozen droplets if phase separation occurs. Figure 32 shows the TGA data obtained from powders derived from the two different solutions. The two curves are virtually identical except that the more dilute solution produces powder having a slightly higher water content. This was reflected in the DTA traces by the water peaks occurring at slightly lower temperatures. It was also found, as shown in Table 6, that the dilute solutions produce a dried powder that develops a slightly higher specific surface area.

SPRAY DRIED $Na_2O.6Al_2O_3$(SULPHATE DERIVED)

In this section of the work, powders were prepared using the solution spray drying and the solution spray freezing-freeze drying techniques using a common starting solution. In this way, it was hoped that the characteristics of the SD powders could be more exactly compared with those of the FD powder. It is important to note therefore that differences between the two powder types should be mainly a result of their physical structure as they are chemically very similar.

Both powders were in the form of spheres after drying with average sizes of 11 and 44 μm for the SD and FD powders respectively. Observations of the dried powders on the optical and scanning electron microscopes showed that the powders had very different physical structures. In the optical microscope, for example, the SD spheres are found to be transparent to light (Fig. 33). When crushed, the spheres break down into numerous small fragments (Fig. 34). In reflected polarised light these fragments give rise to multicoloured fringe patterns, which indicates the fragments are very thin. These observations indicate that the spheres are probably hollow with only a thin shell of material. This was confirmed by viewing the SD powder on the SEM. In Fig. 35, the powder is shown before and after crushing.

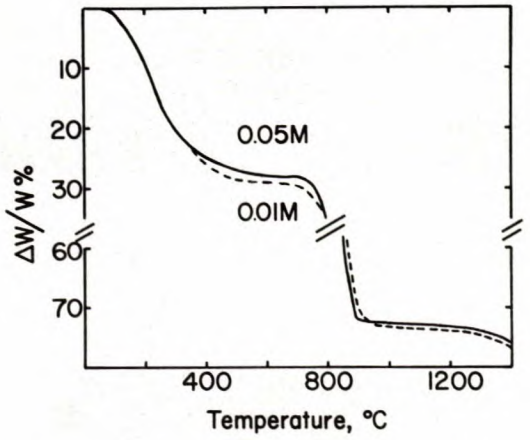

Fig. 32 - TGA of freeze-dried powders derived from solutions of different concentration

Table 6 - Effect of concentration of specific surface area

Calcination temperature (°C)	Specific surface area (m^2/g) 0.05 M	0.01 M
1150	39	52
1200	34	34
1250	16	22
1300	10	14

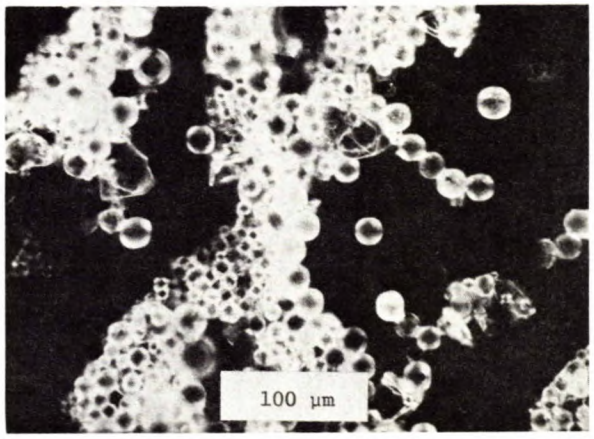

Fig. 33 - Optical micrograph of spray-dried powder viewed under crossed polars

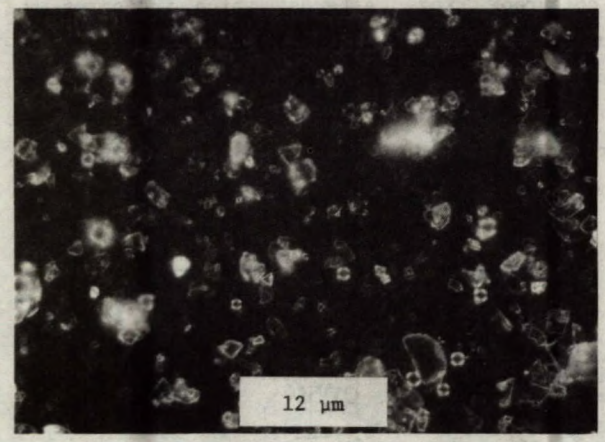

Fig. 34 - Crushed spray-dried powder

(a)

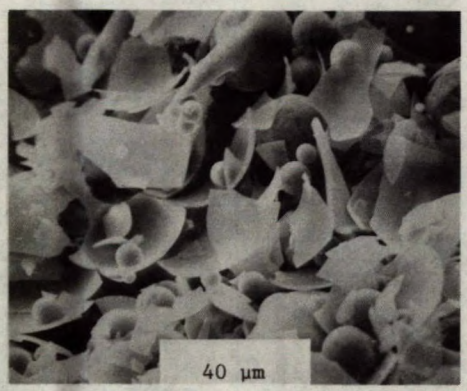

(b)

Fig. 35 - SEM micrographs of spray-dried powder
(a) as-dried, (b) lightly crushed

The wall thickness of the spheres was in the range of 0.1 to 0.5 μm. It appears from these observations that the SD powder is formed in a glass-like state. X-ray diffraction analysis confirmed that the SD products were amorphous. These observations are similar to those of de Lau for spray-dried $Al_2(SO_4)_3$ (74).

The intricate porous nature of the FD spheres was described in the previous section. In this work, however, the FD powder was derived from a more concentrated starting solution. As shown in Fig. 36, this leads to a difference in the form of the porosity in the sphere. In this figure some of the structure within the sphere can be seen. This structure must be formed during the spray freezing-freeze drying process and is typical of dendritic growth, which is probably a result of the formation of ice crystals during freezing. Figure 37 shows the structure within a broken FD sphere in more detail. From these ob-

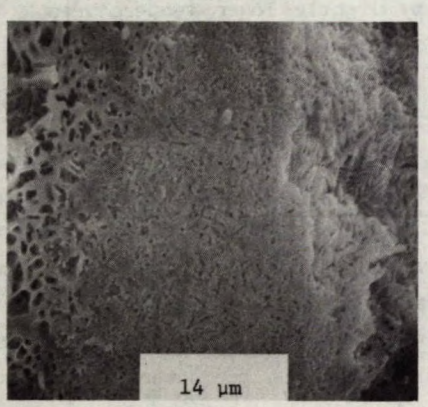

Fig. 36 - Freeze-dried sphere

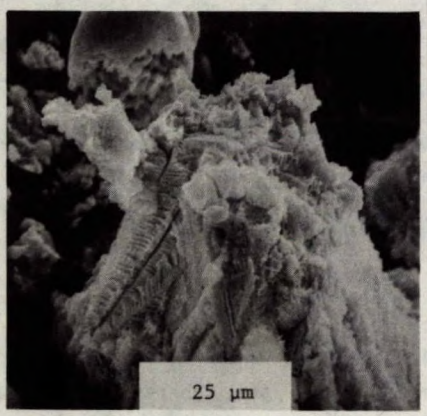

Fig. 37 - Structure within freeze-dried sphere

servations it can be seen that the surface area in the FD powder will be higher than the SD powder and that the porosity distribution is different for the two powder types.

The result of the X-ray diffraction analysis on the calcined powders are summarized in Table 7. The phase sequence is similar to that discussed earlier except for the SD powder, in which α-Al_2O_3 is formed at 1200°C and the final reaction to form the β/β''-Al_2O_3 mixture is slower. The β-Al_2O_3 content of the SD powders is higher than that of the FD powder. Figure 38 compares the X-ray spectra for samples calcined at 1300°C (1 h) to illustrate these points. By 1600°C, the amount of β''-Al_2O_3 has decreased significantly in both types of powder. The transformation was found to be nearer completion in the FD powder. It would appear from these results that the FD powder reacts more readily to form the different phases which is probably due to a better degree of mixing. Included in Table 7 are the approximate f(β) values for the two powders. By sintering an SD powder at 1600°C for 2 h it was possible to obtain a powder containing no β''-Al_2O_3. This sample was used to index the powder pattern of β-Al_2O_3 and Tables 8 and 9 give the data obtained. Table 10 compares the calculated lattice parameters with other data in the literature and in Appendix B, the powder pattern derived from a single crystal study is given.

On heating to 1300°C, both powders undergo approximately 75% weight loss as discussed previously (Fig. 39). The two powders have different water contents after drying so that it is difficult to compare the curves. It was, however, possible from previous data to find an FD powder (0.04 M) with the same water content and the comparison of the weight loss data is given in Fig. 40. In this comparison it is clear that the weight loss characteristics of the two powder types are very similar except that the FD powder loses its water slightly more easily. DTA traces for the FD and SD powders are given as Fig. 41 and 42. The two traces are similar except that the peaks occur at slightly higher temperatures in the SD powder. The origin of the peaks was discussed in the last section.

Figure 43 compares the specific surface areas for the two types of powder during the formation of the β/β''-Al_2O_3 mixture. It can be seen that the SD powder has the lower surface area at a given temperature. This behaviour is probably

Table 7 - Phase sequence for calcined powders

Temperature (°C)	Phases	
	Spray-dried	Freeze-dried
As dried	Amorphous	Amorphous
200	Amorphous	Amorphous
400	$Al_2(SO_4)_3$ + ?	$Al_2(SO_4)_3$ + ?
600	$Al_2(SO_4)_3$ + ?	$Al_2(SO_4)_3$ + ?
900	η-Al_2O_3 + Na_2SO_4	η-Al_2O_3 + Na_2SO_4
1000	η-Al_2O_3 + Na_2SO_4	η-Al_2O_3 + Na_2SO_4
1100	η-Al_2O_3 + Na_2SO_4	η-Al_2O_3 + Na_2SO_4
1200	β/β''-Al_2O_3 + α-Al_2O_3 + Na_2SO_4	β/β''-Al_2O_3 + Na_2SO_4
1300	β/β''-Al_2O_3 + α-Al_2O_3 + Na_2SO_4	β/β''-Al_2O_3
1400	β/β''-Al_2O_3 (0.30)	β/β''-Al_2O_3 (0.34)
1500*	β/β''-Al_2O_3 (0.59)	β/β''-Al_2O_3 (0.55)
1600*	β/β''-Al_2O_3 (0.87)	β/β''-Al_2O_3 (0.82)

* pressed into pellets and protected by powder of same composition

? not enough lines to identify second phase [possibly $NaAl(SO_4)_2$]

f(β) values in brackets

a result of the different porosity distributions in the two types of powder which would be expected to limit crystal growth more in the FD powder.

Because the FD and SD powders have relatively high surface areas it would be expected that loss of soda could be significant in these powders. These results are given in Fig. 44 in terms of the Al/Na ratio. This ratio increases more rapidly for the FD powder at temperatures above about 1350°C. Included in this figure is the S content for the powders. The decrease in S content is associated with the decomposition of Na_2SO_4 which occurs more readily in the FD powder. There is, however, a small percentage of S remaining in the powders even after 1 h at 1400°C. Preliminary vacuum hot-pressing studies of these powders indicated that the presence of this S as Na_2SO_4 leads to fabrication difficulties in which liquid-phase Na_2SO_4 is reduced during pressing to form a sulphide. The sulphide will be present as a second phase, presumably at grain boundaries and will probably give rise to undesirable electrical properties. This problem is not so important during conventional sintering as the higher temperatures will allow the Na_2SO_4 to disappear during densification. To reduce S levels in the calcined powders to those required for hot pressing while retaining a relatively high surface area, it was found necessary to calcine the two powders at 1300°C for 24 h. Such long calcination times give

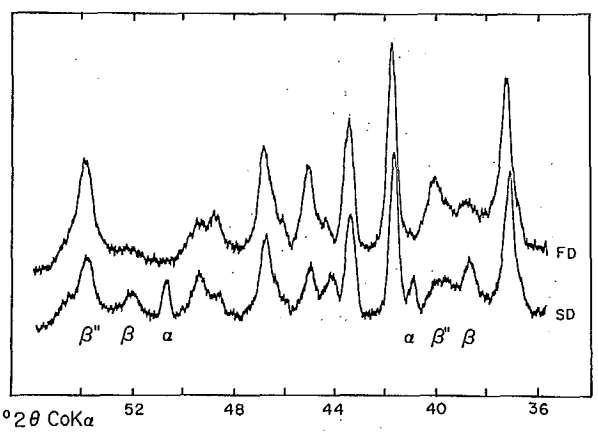

Fig. 38 - Comparison of X-ray diffraction patterns for FD and SD powders (calcined 1300°C, 1 h)

Table 8 - X-ray diffraction data for sodium β-Al_2O_3 (Debye-Scherrer)

Peak	d(Å) meas.	d^{calc}(Å)	hkl	I/Io
1	11.4	11.30	002	100
2	5.67	5.65	004	50
3	4.45	4.46	012	15
4	4.04	4.08	013	10
5	2.80	2.800	110	25
6	2.69	2.688	017	40
7	2.51	2.509	114	35
8	2.42	2.411	020	15
9	2.37	2.371	022	10
10	2.31	2.308	023	5
11	2.247	2.247	116	20
12	2.140	2.137	025	20
13	2.033	2.039	026	25
14	1.940	1.939	027	15
15	1.838	1.840	028	10
16	1.647	1.653	$02\bar{1}0$	10
17	1.591	1.594	127	5
18	1.969	1.568	$02\bar{1}\bar{1}$	15
19	1.566	1.544	034	25
20	1.540	1.538	$01\bar{1}\bar{4}$	5
21	1.485	1.486	036	10
22	1.409	1.412/1.413	$00\bar{1}6/02\bar{1}\bar{3}$	20
23	1.400	1.400	220	45
24	1.357	1.359	224	10
25	1.345	1.344	$02\bar{1}\bar{4}$	10
26	1.240	1.242	317	10
27	1.210	1.211	401	5
28	1.155	1.154	406	5
29	1.136	1.135	047	5
30	1.059	1.058/1.058	$22\bar{1}\bar{4}/410$	10
31	1.052	1.051/1.052	$01\bar{2}\bar{1}/327$	10
32	1.043	1.044	$40\bar{1}\bar{1}$	15
33	1.019	1.019	416	10
34	.9947	.9945	$04\bar{1}\bar{3}$	15
35	.9689	.9695	$04\bar{1}\bar{4}$	10
36	.9289	.9281/.9290	$21\bar{2}\bar{1}/057$	5
37	.9166	.9178	$31\bar{1}\bar{8}$	< 2
38	.9142	.9158	421	5
39	.8984	.8982	425	5

rise to soda loss and hence a loss in compositional control. Table 11 compares the impurity levels for powders calcined under these conditions. The impurity levels are similar for the two powders except for a higher Si content in the FD powder. The origin of this impurity could not be determined but it was still considered to be low enough not to cause concern. It can be seen from

Table 9 - X-ray diffraction for Na β-Al_2O_3 (Guinier)

Peak	d(Å) meas.	d^{calc}(Å)	hkl	I/Io
1	11.2	11.30	002	100
2	5.66	5.65	004	45
3	4.74	4.74	101	5
4	4.47	4.46	102	15
5	4.08	4.08	103	10
6	3.68	3.68	104	< 2
7	2.97	2.975	106	5
8	2.798	2.800	110	25
9	2.679	2.688	107	40
10	2.506	2.509	114	35
11	2.411	2.411	201	30
12	2.374	2.371	202	15
13	2.245	2.247	116	20
14	2.134	2.137	205	25
15	2.033	2.039	206	25
16	1.940	1.939	207	10
17	1.838	1.840	208	5
18	1.589	1.594	217	5
19	1.565	1.568	$20\bar{1}1$	10
20	1.533	1.538	218	5

Table 10 - Lattice parameters for Na β-Al_2O_3

a(Å)	c(Å)	Source
5.60	22.6	This work
5.592	22.61	Dyson and Johnson
5.594	22.53	Peters et al
5.596	22.52	Felsche
5.584	22.45	Beevers and Ross
5.593	22.610	Yamaguchi and Suzuki
5.59	22.49	Théry and Briançon
5.592-5.597	22.46-22.52	Harata

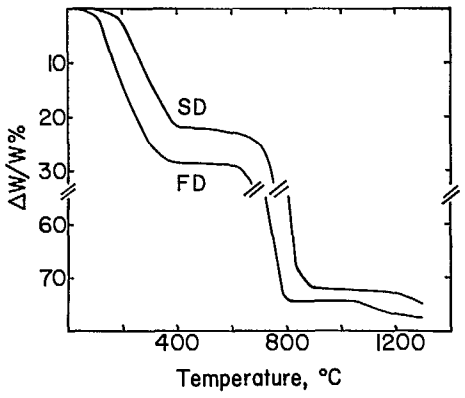

Fig. 39 - TGA for spray-dried (SD) and freeze-dried (FD) powders

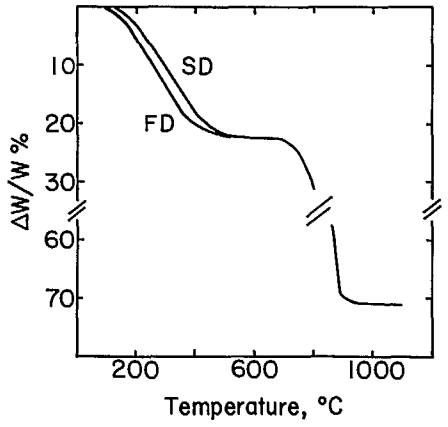

Fig. 40 - TGA for spray-dried (SD) and freeze-dried (FD) powders

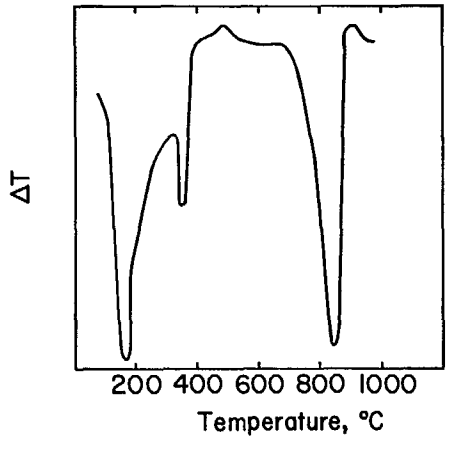

Fig. 41 - DTA of freeze-dried powder

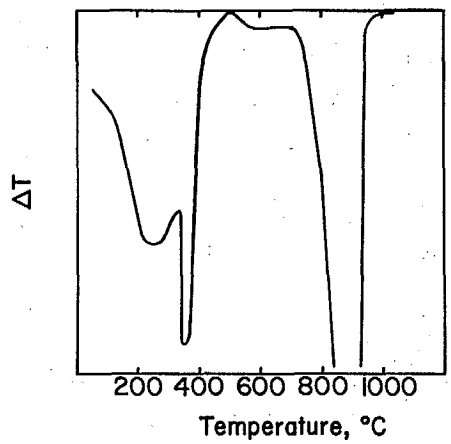

Fig. 42 - DTA of spray-dried powder

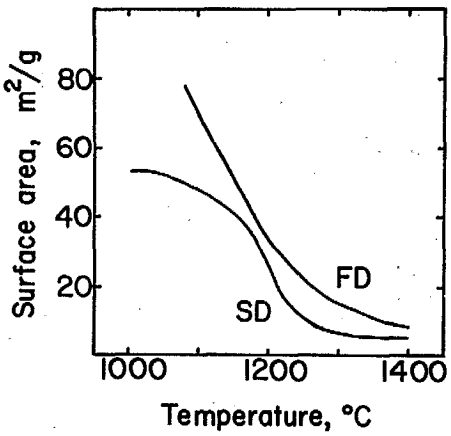

Fig. 43 - Specific surface area developed in spray-dried and freeze-dried powders on calcination for 1 h in air

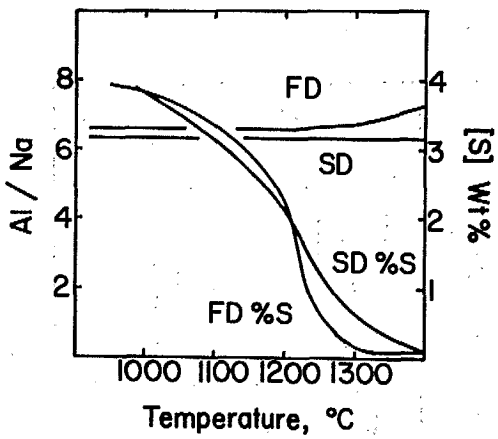

Fig. 44 - Variation of the Al:Na mole ratio and total S content for spray-dried and freeze-dried materials resulting from calcination in air for 1 h

Table 11 - Spectrochemical analysis for calcined SD and FD powders (1300°C, 24 h)

Element	SD (ppm)	FD (ppm)
Si	9	70
Mg	2	2
Mo	100	80
Pb	10	ND
Ga	10	10
Cu	100	90

Elements below detection level: P, Mn, Cr, Zr, Ag, Ni, Sb, Ca, Sn, Ti, Cd, Ba, Be, B, As, W, Nb, Ta, Bi, Ge, V, Li, In, Zn, Co, Sr

ND - Not detected

this data that both the SD and FD techniques give powders of high purity. Figures 45 and 46 are the infrared spectra for the FD and SD powders after calcination at 1300°C for 24 h. Both powders have a significant peak at 3300 cm^{-1}, which indicates that the powders tend to absorb moisture. This moisture must be picked up during storage and handling. It has been suggested by Kummer (4) that the water molecules can enter the Na-containing planes rather than being a result of an ion-exchange process. The rest of the spectra consists of a broad absorption band between 500 and 900 cm^{-1} and peaks at 1460 cm^{-1}, 1150 cm^{-1}, 460 cm^{-1}, 380 cm^{-1} and 315 cm^{-1}. The origin of these peaks has not yet been determined.

The calcined powders were observed in the SEM. The agglomeration between spheres in the FD powder appeared to be more extensive than that observed on FD powder derived from more dilute solutions (Fig. 47). The structure of the FD spheres themselves is a complex aggregation of the ultrafine crystals (Fig. 48). Most of these crystals are equiaxed in agreement with TEM work and appear to have undergone some sintering (Fig. 49). There was, however, evidence of some needle-shaped crystals on the surface of the spheres (Fig. 50). If the powder is gently crushed prior to observation,

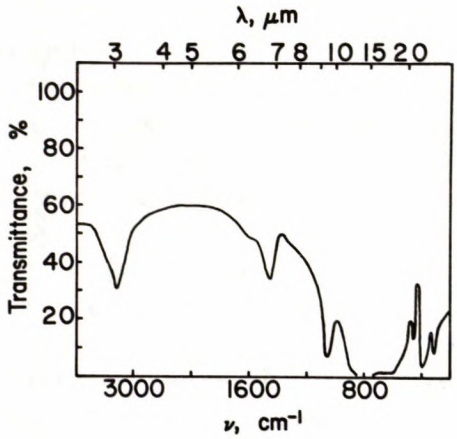

Fig. 45 - Ir spectrum of freeze-dried powder after calcination in air at 1300°C for 24 h

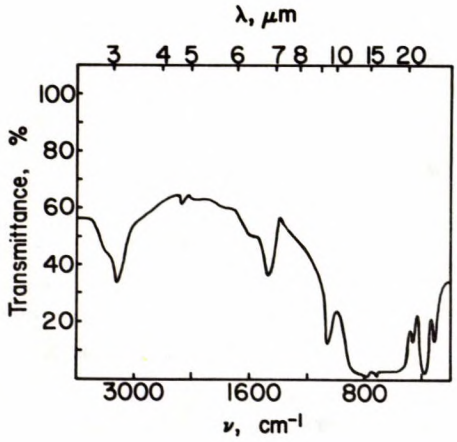

Fig. 46 - Ir spectrum of spray-dried powder after calcination in air at 1300°C for 24 h

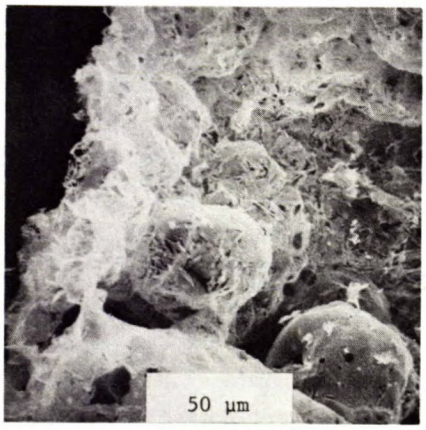

Fig. 47 - Calcined FD spheres (agglomerated)

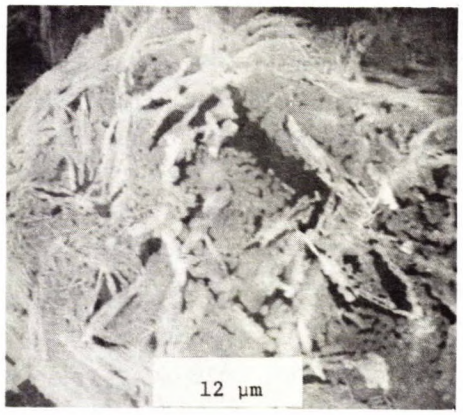

Fig. 48 - Calcined FD sphere

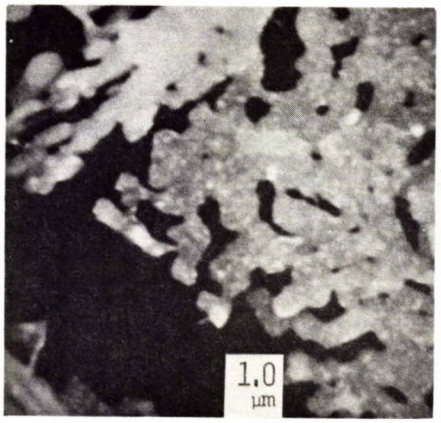

Fig. 49 - Fine, equiaxed crystals formed in FD sphere

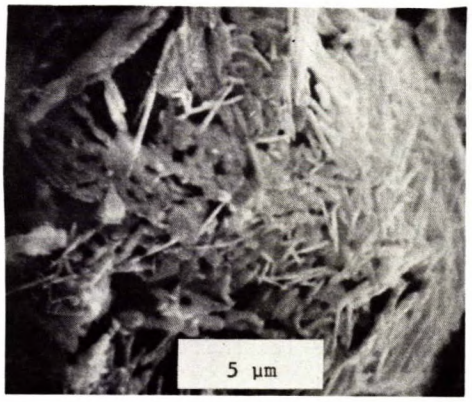

Fig. 50 - Formation of needle-shaped crystals within FD sphere

the spheres break down readily but still in the form of complex agglomerates (Fig. 51). Observation of the SD powder also shows the spherical agglomerates. In this case the surfaces of the spheres (Fig. 52) appear more dense than those of the FD spheres but the material is presumably still contained within a thin shell. The crystals appear to be small equiaxed platelets, but again there was evidence of some needle-shaped crystals in the spheres.

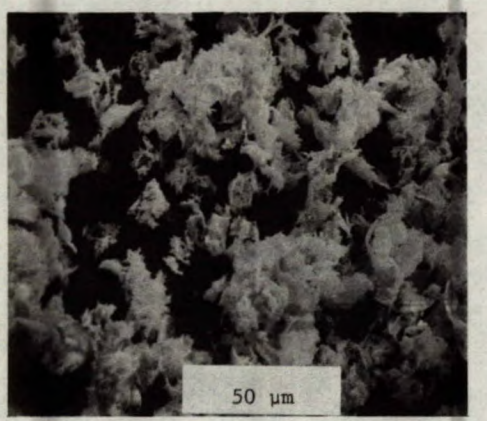

Fig. 51 - Crushed calcined FD powder

Fig. 52 - Calcined SD powder

SPRAY DRIED $Na_2O.6Al_2O_3$ (NITRATE DERIVED)

As pointed out earlier, the starting solution for spray-dried powders could also be based on $Al(NO_3)_3$ rather than on $Al_2(SO_4)_3$. Both these salts are highly soluble in water but the nitrate-derived powders would clearly have some advantages over those based on sulphate solutions. For example, both $Al(NO_3)_3$ and $NaNO_3$ decompose at relatively low temperatures of 150°C and 380°C, respectively, which therefore offers the opportunity of lower calcination temperatures for total decomposition. Furthermore, the absence of a salt which is stable to high temperatures such as Na_2SO_4 in the case of the sulphur derived powders should simplify the formation of β- or β"-Al_2O_3. As noted earlier, the technique of freeze drying could not be used for the nitrate solutions but, in the case of spray drying, powders could be successfully produced.

As shown in Fig. 53, the powder is in the form of opaque spheres which have a tendency to agglomerate even after drying.

In the SEM observations (Fig. 54), the spheres have a rough texture with a crystalline phase, probably $NaNO_3$, on the outside surface. From the broken sphere in Fig. 55, it would appear they are also hollow.

The sequence of phase formation during calcination of the nitrate-derived powders is given in Table 12 and contrasts quite dramatically with that of the spray-dried powders discussed earlier. After drying, the powder contains only $NaNO_3$ as a crystalline phase. The $Al(NO_3)_3.9H_2O$ has presumably decomposed to some amorphous phase. By 400°C the $NaNO_3$ has also decomposed so that the powder is amorphous to X-rays. This continues until 1000°C when λ- and β-Al_2O_3 are present. The transformation of λ- to β"-Al_2O_3 occurs over a wide range of temperatures until at 1300°C, the powder is a mixture of β- and β"-Al_2O_3. TGA indicates that the powder reaches constant weight by about 800°C (Fig. 56). The DTA trace in Fig. 57 shows a broad endothermic peak between 100 and 600°C. It would be expected that this peak may result from water loss, $NaNO_3$ melting, and decomposition. An exothermic peak at 860°C is probably related to the formation of λ- or β-Al_2O_3.

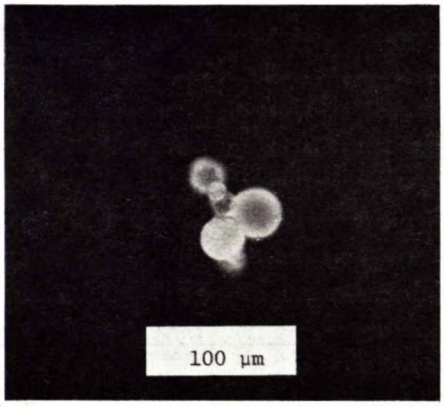

Fig. 53 - Spray-dried powder (nitrate solution) viewed in reflected polarized light

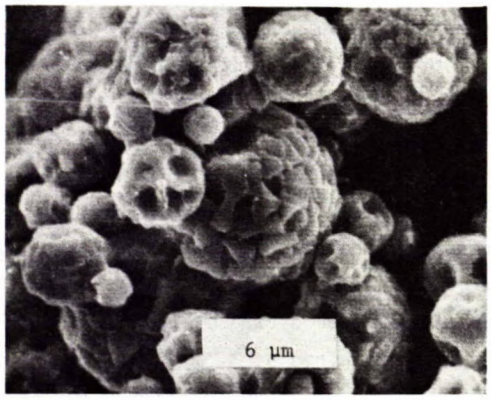

Fig. 54 - SEM micrograph of spray-dried powder (nitrate solution)

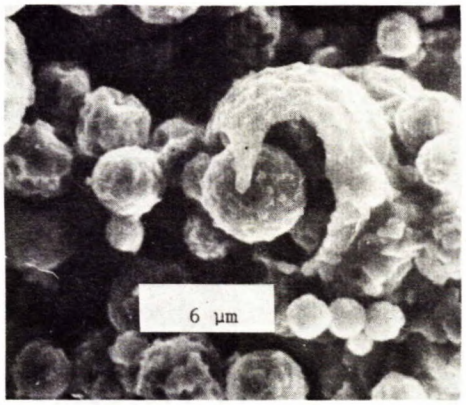

Fig. 55 - SEM micrograph of spray-dried powder (nitrate solution) showing the presence of hollow spheres

After decomposition the specific surface area of the powder drops rapidly, as shown in Table 13. At temperatures below 1000°C the surface area of the powders is relatively high with an equivalent spherical diameter of less than 2 µm.

Chemical analyses for sodium are given in Table 14 as a function of calcination temperature. These results again show some sodium loss above 1200°C. Again it is not clear why the Na_2O contents are low but it was suspected that this was a result of inaccuracy in the analysis.

Table 12 - Phase sequence of spray-dried nitrate powder compared with spray-dried sulphate powder

Temperature (°C)	Spray-dried sulphate	Spray-dried nitrate
As prepared	Amorphous	$NaNO_3$
200	Amorphous	$NaNO_3$
400	$Al_2(SO_4)_3$ + ?	Amorphous
600	$Al_2(SO_4)_3$ + ?	Amorphous
800	-----	Amorphous
900	η-Al_2O_3 + Na_2SO_4	-----
1000	η-Al_2O_3 + Na_2SO_4	λ-Al_2O_3, β-Al_2O_3
1100	η-Al_2O_3 + Na_2SO_4	λ-, β-, β"-Al_2O_3
1200	β/β"-Al_2O_3 + α-Al_2O_3 + Na_2SO_4	β + β"-Al_2O_3 + λ-Al_2O_3(tr)
1300	β/β"-Al_2O_3 + α-Al_2O_3 + Na_2SO_4	β + β"-Al_2O_3
1400	β + β"-Al_2O_3	β + β"-Al_2O_3
1500*	β + β"-Al_2O_3	β + β"-Al_2O_3
1600*	β + β"-Al_2O_3	β + β"-Al_2O_3

? unidentified phase, possibly $NaAl(SO_4)_2$

* Calcined as-pressed disc covered by powder of same composition

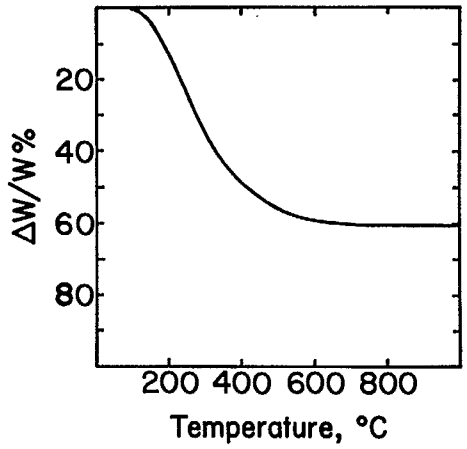

Fig. 56 - TGA of spray-dried powder derived from nitrate solution

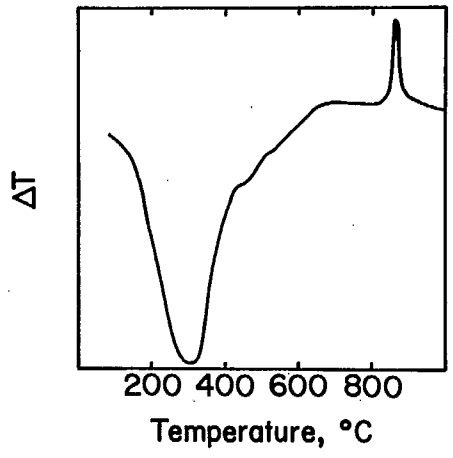

Fig. 57 - DTA of spray-dried powder derived from nitrate solution

Table 13 - Specific surface area for spray-dried nitrate powder

Temperature (°C)	Specific surface area (m^2/g)
800	36.9
900	26.9
1000	1.08
1100	0.78
1200	0.71
1300	0.61

Table 14 - Chemical analysis for spray-dried nitrate powder

Calcination temperature	Na_2O (wt %)
1000	7.32
1100	7.53
1200	7.49
1300	7.18
1400	7.20

Finally the powders were observed after calcination. In contrast to the sulphate-derived powders, these were found to have a hard, granular nature after calcination possibly due to some melting process. At 1000°C, however, very fine platelet crystals were observed that were similar to those observed for the spray-dried sulphate powders. These crystals were again in the form of complex aggregates often retaining the spherical nature of the dried powder. At higher temperatures, long thin needle-shaped crystals are formed. Figure 58 shows this type of behaviour for a powder calcined at 1350°C. At higher magnifications, it can be seen that these needle-shaped crystals are very thin. It was also found that the calcined aggregates did not break down readily under stress.

CONCLUSIONS

FREEZE-DRIED $Na_2O.6Al_2O_3$

The dried powder consisted of spheres having complex pore structures. After drying, the powders were amorphous with respect to X-ray diffraction and had a tendency to absorb moisture from the atmosphere. The water content was also found to depend on the drying conditions.

During calcination the powder crystallizes and then at higher temperatures separates into two distinct phases, one of which (Na_2SO_4) is probably present as a liquid. This would indicate that the homogeneity of the powder tends to be lost during calcination.

Above 1250°C, sodium β"-Al_2O_3 is formed which transforms slowly into β-Al_2O_3 at higher

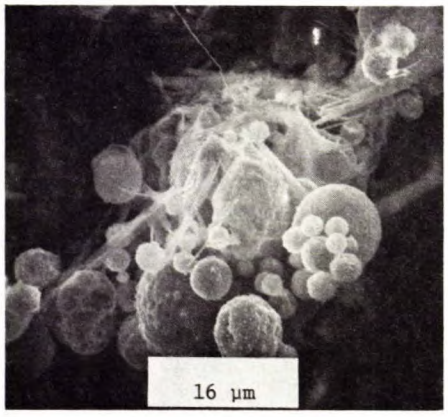

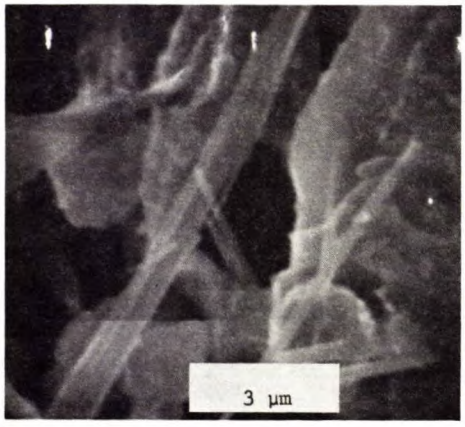

Fig. 58 - SEM micrographs of spray-dried powder derived from a nitrate solution and calcined in air at 1350°C

temperatures. Both phases were found to co-exist in the temperature range of 1300 to 1650°C. Some powder agglomeration was observed during calcination but it was found that these agglomerates break down readily under low stresses. The formation of β''-Al_2O_3 is accompanied by rapid decrease in the specific surface area of the powder and, at temperatures above about 1350°C, chemical analysis indicates that sodium is lost from the powders.

The calcined powder still retained the spherical nature of the dried powder but it was found that the spheres consisted of complex aggregates of very fine crystals, the majority of which were in the form of equiaxed platelets.

Freeze-dried powders were also produced using a variety of sodium salts for the starting solution, but the choice of salt did not appear to alter the powder characteristics in any major way. Attempts to use $Al(NO_3)_3$ instead of $Al_2(SO_4)_3$ proved unsuccessful. Changes in the concentration of the starting solution were also studied and it was found that the more dilute solutions had slightly higher surface areas, lost water more rapidly, and had different structures within the dried spheres.

SPRAY-DRIED $Na_2O.6Al_2O_3$ (SULPHATE DERIVED)

Powders were produced from a common solution by both the spray-drying and freeze-drying techniques. The two powder types were found to have very different physical structures after drying. The SD powder was in the form of fine optically transparent hollow spheres in comparison with the porous nature of the FD spheres.

During calcination, the SD powder has a tendency to form α-Al_2O_3, does not decompose into β''-Al_2O_3 until slightly higher temperatures and has slightly less β''-Al_2O_3 than the FD powder. The specific surface area of the SD powder was found to be slightly less than that of the FD powder. This effect would be expected, not only from the initial observation of the two powder types but also as the extensive porosity in the FD spheres would be expected to limit crystal growth. The SD powder does not lose sodium as rapidly as the FD powder. Comparison of the impurity levels of the two powders indicated that they were within tolerable limits.

It was found from ir spectroscopy that both the FD and SD powders contained some water even after calcination, presumably absorbed from the atmosphere. Observations of the calcined SD powder indicated that these spheres also consisted of complex aggregates of fine crystals.

SPRAY-DRIED $Na_2O.6Al_2O_3$ (NITRATE DERIVED)

These powders were in the form of opaque hollow spheres after drying, with evidence of a crystalline phase on the surface of the spheres ($NaNO_3$). The powders were somewhat agglomerated after drying. The sequence of phases formed during calcination of this powder contrasts significantly with that of the sulphate-derived powders

in that decomposition occurs at a lower temperature and that λ-Al_2O_3 is formed as a transition phase at about 900°C. At approximately 1300°C the λ-Al_2O_3 has disappeared and the powder becomes a mixture of β- and β"-Al_2O_3. After decomposition, the specific surface area of the powder drops rapidly, so that above 1000°C, it is less than 1 m^2/g.

Observations on powders calcined at 1000°C showed the presence of platelet crystals but, at higher temperatures long needle-shaped crystals were also present. The nitrate-derived powder was hard and granular after calcination and did not break down readily under stress. Chemical analysis indicated that sodium is lost from the powders above about 1200°C.

ACKNOWLEDGEMENTS

The authors would like to acknowledge the technical assistance of A.J. Hanson, S. Hutchison and G.A. Johnson, the work of I. Szymanski in computing the powder diffraction patterns and staff of the Chemical Analytical Laboratory of CANMET, for providing the chemical analyses.

REFERENCES

1. Holzäpfel G. and Rickert H. "Solid state electrochemistry - new possibilities for research and industry"; Naturwiss.; 64:2:53-58; 1977.

2. Steele, B. "Ions in the solid state"; New Scientist; 78:705-707; 1978.

3. Wheat, T.A. "Exploring ionic conductors"; Clay and Ceramics; 52:1:17-22; 1979.

4. Kummer, J.T. "β-alumina electrolytes"; Prog in Solid State Chem.; 7:141-175; 1972.

5. Whittingham, M.S. and Huggins, R.A. "Beta-alumina - prelude to a revolution in solid state chemistry", Solid State Chemistry; NBS Spec. Publ. 364; NBS, Washington, D.C., 139-154; July 1977.

6. Robinson, A.L. "Advanced storage batteries; progress but not electrifying"; Science; 192: 541; 1976.

7. Gordon, R.S. "Ceramics in the sodium-sulphur battery", Ceramics for Energy Applications; Workshop at Battelle Columbus Labs, Columbus, Ohio; November 1975.

8. Stansell, J. "Sodium-sulphur: a battery of problems and hopes"; Science; 78:420-421; February 1978.

9. Powers, R.W. and Mitoff, S.P. "An analysis of the impedance of polycrystalline beta-alumina"; J Electrochem Soc; 122:2:226-231; 1975.

10. Virkar, A.V., Miller, G.R. and Gordon, R.S. "Resisitivity - microstructure relations in lithia-stabilized β"-alumina"; J Am Ceram Soc; 61:5-6:250-252; 1978.

11. DeJonghe, L.C. "Grain boundaries and ionic conduction in sodium beta-alumina"; J Mater Sci; 14:33-48; 1979.

12. Tennenhouse, G.J., Ku, R.C., Richman, R.H. and Whalen, T.J. "Deterioration in ceramic electrolytes for sodium-sulphur batteries"; Am Ceram Soc Bull; 54:5:523-27:531; 1975.

13. Stoddart, C.T.H. and Hondros, E.D. "Auger electron spectroscopy of β"-alumina electrolyte"; Proc Brit Ceram Soc; 73:61-64; 1974.

14. Demott, D.S. and Redfern, B.A.W. "The deterioration of beta-alumina during electrolysis"; Journal de Physique; 37:C7:423-27; 1976.

15. Hames, M.D. and Duncan, J.H. "The function and performance of beta-alumina in sodium/sulphur cells"; Society of Automotive Engineers Congress and Exposition, Detroit, Michigan; Paper 750375; February 1975.

16. DeJonghe, L.C., Feldman, L. and Millett, P. "Some geometrical aspects of breakdown of sodium beta-alumina"; Mat Res Bull; 14:589-595; 1979.

17. Armstrong, R.D., Dickinson, T. and Turner, J. "The breakdown of β-alumina ceramic electrolyte"; Electrochim Acta; 19:187-192; 1974.

18. Richman, R.H. and Tennenhouse, G.J. "A model for degradation of ceramic electrolytes in Na-S batteries"; J Am Ceram Soc; 58:1-2:63-67; 1975.

19. Shetty, D.K., Virkar, A.V. and Gordon, R.S. "Electrolytic degradation of lithia-stabilized β"-alumina"; Fracture Mechanics of Ceramics, Vol 4; Edited by R.C. Bradt et al; Plenum Press, New York-London; pp 651-665; 1978.

20. "Research on electrodes and electrolyte for the Ford sodium-sulphur battery"; Annual Report; Contract No. NSF-C805; June 1975.

21. Lazennec, Y., Lasne, C., Margohn, P., and Fally, J. "Factors influencing the lifetime of a pure beta-alumina electrolyte"; J Electrochem Soc; 122:6:734-37; 1975.

22. Yasui, I. and Doremus, R.H. "Non-uniformity of potassium ions in β"-alumina ceramics"; J Am Ceram Soc; 60:7-8;296-301; 1977.

23. Bragg, W.L., Gottfried, C., and West, J. "Structure of β-alumina"; Z Krist; 77:255; 1931.

24. Beevers, C.A. and Ross, M.A. "Crystal structure of beta-alumina, $Na_2O.11Al_2O_3$"; Z Krist; 97:59; 1937.

25. Peters, C.R., Bettman, M., Moore, J.W., and Glick, M.D. "Refinement of the structure of sodium β-alumina"; Acta Cryst; B27:1826-1833; 1971.

26. Yamaguchi, G. and Suzuki, K. "On the structure of alkali polyaluminates"; Bull Chem Soc Japan; 41:93-99; 1968.

27. Théry, J. and Briançon, D. "Structure et propriétés des aluminates de sodium"; Rev Hautes Tempér et Réfract; 1:221-27; 1964.

28. Bettman, M. and Peters, C.R. "The crystal structure of $Na_2O.MgO.5Al_2O_3$ with reference to $Na_2O.5Al_2O_3$ and other isotypal compounds"; J Phys Chem; 73:6:1774-80; 1969.

29. Dyson, D.J. and Johnson, W. "The identification of β-alumina type phases"; Trans Brit Ceram Soc; 72:49-55; 1973

30. Harata, M. "Lattice constants of non-stoichiometric beta-alumina"; Mat Res Bull; 6:461-64; 1971.

31. Ray, A.K. and Subbarao, E.C. "Synthesis of sodium β and β" alumina"; Mat Res Bull; 10: 583-590; 1975.

32. Morgan, P.E.D. "Low temperature synthetic studies of beta-aluminas"; Mat Res Bull; 11: 233-242; 1976.

33. Fally, J., Lasne, C., Lazennec, Y., LeCars, Y. and Margohn, P. "Study of a beta-alumina electrolyte for sodium-sulphur battery"; J Electrochem Soc, 120:10:1296-98; 1973.

34. Bevan, D.J.M., Hudson, B., and Moseley, P.T. "Intergrowth of crystal structures in β-alumina"; Mat Res Bull; 9:1075-1084; 1974.

35. DeJonghe, L.C. "Planar [00.ℓ] disorder in sodium beta-alumina"; J Mater Sci; 12:497-502; 1977.

36. Rolin, M. and Thanh, P.H. "Phase diagrams of non-reactive mixtures with Molybdenum I"; Bull Soc Chim France; 1030-35; 1963.

37. DeVries, R.C. and Roth, W.L. "Critical evaluation of the literature data on beta-alumina and related phases. I, Phase equilibria and characterization of beta-alumina phases"; J Am Ceram Soc; 52:7:364-69; 1969.

38. Weber, N. and Venero, A. Paper 5-J1-70, Annual Meeting of Am Ceram Soc; Philadelphia; May 1970.

39. Weber, N. and Venero, A., Paper 1-JV-70, Annual Meeting of Am Ceram Soc; Philadelphia; May 1970.

40. Boilot, J.P. and Théry, J. "Influence de l'addition d'ion étrangers sur la stabilité relative et la conductivité électrique des phases du type alumine β et β""; Mat Res Bull; 11:407-414; 1976.

41. Youngblood, G.E., Virkar, A.V., Cannon, W.R. and Gordon, R.S. "Sintering processes and heat treatment schedules for conductive lithia-stabilized β"-Al_2O_3"; Am Ceram Soc Bull; 56:2:206-210:212; 1977.

42. Kennedy, J.H. and Sammells, A.F. "Conductivity of beta-alumina and its dependence on sodium and magnesium content"; J Electrochem Soc; 119:1609; 1972.

43. Kennedy, J.H. and Ackridge, J.R. "Inhibition of sintering of β-Al_2O_3 by V_2O_5"; J Am Ceram Soc; 59:5-6:279-80; 1976.

44. Elliot, A.G. and Huggins, R.A. "Phases in the system $NaAlO_2$-Al_2O_3"; J Am Ceram Soc; 58:11-12:497-500; 1975.

45. Wynn Jones, I. and Miles, L.J. "Production of β-Al_2O_3 electrolyte"; Proc Brit Ceram Soc; 19: 161-178; 1969.

46. Francis, T.L., Phelps, F.E. and MacZura, G. "Sintered sodium beta alumina ceramics"; Am Ceram Soc Bull; 50:7:615-19; 1971.

47. Chatterji, D. "Development of sodium-sulphur batteries for utility application"; EPRI EM-266, Project 128-3; Annual Report; December 1976.

48. DeJonghe, L.C. and Chandan, H. "Improving the sintering behaviour of sodium β-alumina"; Am Ceram Soc Bull; 55:3:312-13; 1976.

49. Weiner, S.A. and Tischer, R.P. "Research on electrodes and electrolytes for the Ford sodium-sulphur battery"; Annual Report, Contract NSF-C805; July 1976.

50. May, G.J. and Hooper, A. "The effect of microstructure and phase composition on the ionic conductivity of magnesium-doped sodium beta-alumina"; J Mater Sci; 13:1420-86; 1978.

51. Chowdhry, U. and Cannon, R.M. "Microstructural evolution during the processing of sodium β-alumina"; Processing of Polycrystalline Ceramics, Edited by H. Palmour III, R.F. Davis, and T.M. Hare; Plenum Press, New York; 443-455; 1978.

52. Powers, R.W. "The electrophoretic forming of beta-alumina ceramics"; J Electrochem Soc; 122:4:490-500; 1975.

53. Kennedy, J.H. and Foissy, A. "Fabrication of beta-alumina by electrophoretic deposition from suspensions in dichloromethane"; J Electrochem Soc; 122:4:482-86; 1975.

54. Byckalo, W., Rosenblatt, G. Lam, J., and Nicholson, P.S. "Slip casting of β-Al_2O_3 for alkali probes in molten metals"; Am Ceram Soc Bull; 56:286-88; 1976.

55. Rivier, M. and Pelton, A.D. "A new slip-casting technique for the laboratory fabrication of β-alumina and other ceramics"; Am Ceram Soc Bull; 57:2:183-85; 1978.

56. Virkar, A.V., Tennenhouse, G.J. and Gordon, R.S. "Hot-pressing of Li_2O-stabilized β"-alumina"; J Am Ceram Soc; 57:11:508; 1974.

57. Sarian, S., Dunbar, B.J. and McEntee, W.J. "Effect of microstructure on Na^+ diffusion in beta-alumina"; Ceramic Microstructure '76, edited by R.M. Fulrath and J.A Park; Westview Press, Boulder, Colorado; 621-632; 1977.

58. Babini, G.N., Bellosi, A. and Vincenzini, P. "Densification kinetics of vacuum hot-pressed sodium beta-aluminas"; Ceramurgia International; 3:4:147-151; 1977.

59. McDonough, N.J., Flinn, D.R., Stern, K.H. and Rice, R.W. "Hot pressing and physical properties of Na beta-alumina"; J Mater Sci; 13: 2403-12; 1978.

60. Youngblood, G.E. and Gordon, R.S. "Texture-conductivity relationships in polycrystalline lithia-stabilized β"-alumina"; Ceramurgia International; 4:3:93-98; 1978.

61. Ohta, T., Harata, M. and Imai, A. "Preferred orientation in beta-alumina ceramics"; Mat Res Bull; 11:1343-1350; 1976.

62. Powers, R.W. and Mitoff, S.P. "An effect of furnace atmospheres on the sintering of beta-alumina"; Am Ceram Soc Bull; 57:456:458; 1978.

63. Powers, R.N. and Mitoff, S.P. "The influence of crystal structure and of microstructure on some properties of polycrystalline beta-alumina"; Solid Electrolytes, Ed. by P. Hagenmuller and W. Van Gool, Academic Press, New York; 1977.

64. Schnettler, F.J., Monforte, F.R., and Rhodes, W.W. "A cryochemical method for preparing ceramic materials"; Science of Ceramics; Ed. by G.H. Stewart; British Ceramic Society; 4: 79-90; 1968.

65. Paulus, M. "Physical and chemical parameters controlling the homogeneity of fine grained powders and sintering materials"; Processing of crystalline ceramics, Ed. by H. Palmer III, R.F. Davis and T.M. Hare, Plenum Press, New York; 17-31; 1978.

66. Jaeger, R.E., Miller, T.J. and Williams, J.C. "Effects of ammonium hydroxide on phase separation in the cryochemical processing of salt solutions"; Am Ceram Soc Bull; 53:12:850-52; 1974.

67. Druzhinin, I.G. and Gorbunov, V.D. "Polytherm of solubility of the system aluminum sulphate - sodium sulphate - water from -10 to 95°"; Izv Akad Nauk Kirg SSR, Ser Estestv Tekhn Nauk; 4:9:111-21; 1962.

68. Thomson Jr., J. "Chemical preparation of PLZT powders from aqueous nitrate solutions"; Am Ceram Soc Bull; 53:5:421-33; 1974.

69. Tseung, A.C.C. and Bevan, H.G. "Preparation and characterization of high surface area semi conducting oxides"; J Mater Sci; 5:604-10; 1970.

70. Johnson, D.W. and Schnettler, F.J. "Characterization of freeze-dried Al_2O_3 and Fe_2O_3"; J Am Ceram Soc; 53:8:440-44; 1970.

71. King, W.J. and Tseung, A.C.C. "The reduction of oxygen on nickel-cobalt oxides-I"; Electro-

chim Acta; 19:485-91; 1974.

72. Johnson, D.W. Jr., Gallagher, P.K., Schrey, F. and Rhodes, W.W. "Preparation of high surface area substituted $LaMnO_3$ catalysts"; Am Ceram Soc Bull; 55:5:520-23, 527; 1976.

73. Roy, D.M., Neurgaonkar, R.R., O'Holleran, T.P. and Roy, R. "Preparation of the fine oxide powders by evaporative decomposition of solutions"; Am Ceram Soc Bull; 56:11:1023-24; 1977.

74. deLau, J.G.M. "Preparation of ceramic powders from sulphate solutions by spray drying and spray roasting"; Am Ceram Soc Bull; 49:6:572-574; 1970.

75. Akashi, T., Tsuji, T. and Onada, Y. "Sintering of ferrite powder prepared by a new spray-roasting technique"; Sintering and related phenomena; Ed. by G.C. Kuczynski, N.A. Hooton and C.F. Gibbon; Gordon and Breach, New York; 747-58; 1967.

76. Pesher, P. and Pecheva, M. "Preparation of spinel lithium ferrite by thermal treatment of spray-dried formates"; Mat Res Bull; 13: 1167-74; 1978.

77. Ruthier, M.J. "Preparation and sintering characteristics of MgO, Al_2O_3, $MgAl_2O_4$ and $MgCr_2O_4$"; Third. Round Table Meeting; International team for studying sintering; Heraeg-Novi, Yugoslavia; 1973.

78. Gallagher, P.K., Johnson, D.W. Jr., Schrey, F. and Nitte, D.J. "Preparation and characterization of iron oxides"; Am Ceram Soc Bull; 52: 11:842-49; 1973.

79. Mirkovich, V.V. and Wheat, T.A. "Use of liquid nitrogen in spray freezing"; Am Ceram Soc Bull; 49:724-5; 1970.

80. Chemical Engineering Handbook; Ed. by R.H. Perry and C.H. Chilton; McGraw-Hill; New York; 5th Edition; 18:58-63; 1973.

81. Nakamoto, K. "Infrared and raman spectra of inorganic and coordination compounds"; J Wiley and Sons, New York; 239-42; 1978.

82. Fedoror, P.I. and Chih-Yuh, C. "The Al^{3+}, Na^+ Ω SO_4^{2-} system"; Russ J Inorg Chem; 11:3:362-63; 1966.

83. LeCars, Y., Théry, J. and Collongues, R. "Domaine d'existence et stabilité des alumines β et β" dans le system Al_2O_3-Na_2O. Etude par rayons X et microscopie électronique"; Rev Int Hautes Tempér et Refract; 9:153-160; 1972.

84. Morrison, A.D., Stormont, R.W. and Cocks, F.H. "Edge-defined film-fed growth of β-alumina and Mg-substituted β-alumina"; J Am Ceram Soc; 58: 1-2:41-48; 1975.

APPENDIX A

X-RAY POWDER DIFFRACTION DATA FROM SODIUM BETA"-ALUMINA

Powder diffraction pattern for sodium beta"-alumina (MgO-stabilized) calculated from observations of Bettman and Peters (J. Phys. Chem. 73 1774; 1969). The structure factors were obtained from a private communication with M. Bettman, Ford Motor Company.

Table A-1 - Calculated X-ray powder diffraction pattern for sodium beta"-alumina*

Beta"-alumina, Co Radiation, No absorption, Cauchy P.W. = 0.25 at 40 deg.

Sort No.	h	k	l	d Space	Wave length	Rel. I(obs)	Rel. I(cal)	Two Theta
1	0	0	3	11.2833	β	1	1	8.24
2	0	0	3	11.2833		100	100	9.10
3	0	0	6	5.6417		52	35	18.26
4	0	1	2	4.6729		9	5	22.09
5	1	0	4	4.2157		20	14	24.52
6	0	1	5	3.9490		2	1	26.20
7	1	0	7	3.4286		1	1	30.27
8	0	0	12	2.8208		5	5	37.00
9	1	1	0	2.8070		25	20	37.19
10	1	0	10	2.7780		25	23	37.59
11	0	1	11	2.6002		27	35	40.27
12	1	1	6	2.5131		43	41	41.73
13	0	2	1	2.4247		17	16	43.33
14	2	0	2	2.4062		4	2	43.68
15	0	2	4	2.3364		23	22	45.05
16	2	0	5	2.2879		7	4	46.06
17	0	0	15	2.2567		4	4	46.74
18	1	1	9	2.2496		17	13	46.89
19	0	2	7	2.1719		11	12	48.68
20	0	1	14	2.1649		4	4	48.84
21	2	0	8	2.1078		2	2	50.26
22	0	2	10	1.9745		43	50	53.91
23	1	0	16	1.9399		1	1	54.96
24	2	0	11	1.9075		1	1	55.97
25	2	1	1	1.8349		1	1	58.39
26	1	2	2	1.8269		1	1	58.68
27	2	1	4	1.7958		1	1	59.80
28	0	2	13	1.7769		1	1	60.50
29	1	2	5	1.7734		1	0	60.63
30	1	1	15	1.7588		2	2	61.19
31	2	1	7	1.7178		1	1	62.81

* These computations were performed by Dr. Szymanski, Mineral Sciences Laboratories, CANMET.

Table A-1 (cont'd)

Beta"-alumina, Co Radiation, No absorption, Cauchy P.W. = 0.25 at 40 deg.

Sort No.	h	k	l	d Space	Wave length	Rel. I(obs)	Rel. I(cal)	Two Theta
32	2	0	14	1.7143		1	1	62.95
33	1	0	19	1.6728		1	1	64.70
34	3	0	0	1.6206		3	2	67.05
35	2	1	10	1.6150		8	9	67.32
36	0	0	21	1.6119		2	2	67.46
37	0	1	20	1.5984		1	1	68.11
38	0	2	16	1.5959		9	12	68.23
39	1	2	11	1.5777		15	13	69.13
40	1	1	18	1.5623		3	4	69.91
41	3	0	6	1.5576		2	2	70.15
42	0	3	6	1.5576		4	5	70.15
43	2	0	17	0.5404		6	8	71.05
44	3	0	9	1.4883		2	2	73.94
45	0	3	9	1.4883		4	3	73.94
46	1	2	14	1.4630		4	5	75.44
47	0	2	19	1.4370		3	3	77.06
48	0	1	23	1.4086		1	1	78.91
49	2	2	0	1.4035		30	37	79.25
50	2	2	3	1.3928		5	4	79.98
51	2	0	20	1.3890		22	31	80.24
52	2	1	16	1.3873		1	2	80.36
53	2	2	6	1.3620		6	5	82.17
54	1	3	4	1.3316		1	1	84.47
55	3	1	5	1.3225		1	0	85.20
56	0	2	22	1.3001		4	3	87.02
57	1	1	24	1.2603		1	1	90.51
58	2	0	23	1.2590		1	1	90.63
59	0	1	26	1.2576		1	1	90.75
60	2	2	12	1.2566		1	1	90.85
61	0	0	27	1.2537		1	1	91.12
62	1	3	10	1.2527		3	4	91.21
63	1	2	20	1.2449		1	1	91.94
64	3	1	11	1.2351		5	4	92.89
65	3	0	18	1.2277		1	1	93.63
66	4	0	1	1.2147	A1	2	2	94.85
67	4	0	1	1.2147	A2	1	1	95.12
68	4	0	4	1.2031	A1	2	1	96.05
69	4	0	4	1.2031	A2	1	1	96.33
70	4	0	7	1.1788	A1	1	1	98.71
71	3	1	14	1.1777	A1	1	1	98.84
72	2	0	26	1.1477	A1	2	2	102.40
73	2	0	26	2.1477	A2	1	1	102.71

Table A-1 (cont'd)

Beta"-alumina, Co Radiation, No absorption, Cauchy P.W. = 0.25 at 40 deg.

Sort No.	h	k	l	d Space	Wave length	Rel. I(obs)	Rel. I(cal)	Two Theta
74	4	0	10	1.1440	A1	3	4	102.87
75	4	0	10	1.1440	A2	2	2	103.18
76	0	1	29	1.1350	A1	1	1	104.01
77	0	0	30	1.1283	A1	1	1	104.88
78	3	2	4	1.1058	A1	1	1	107.97
79	0	2	28	1.0825	A1	1	1	111.45
80	1	0	31	1.0654	A1	2	2	114.19
81	1	0	31	1.0654	A2	1	1	114.57
82	1	2	26	1.0623	A1	1	1	114.70
83	4	1	0	1.0609	A1	1	1	114.93
84	3	2	10	1.0594	A1	2	2	115.20
85	4	1	0	1.0609	A2	1	0	115.32
86	2	2	21	1.0585	A1	2	3	115.35
87	3	2	10	1.0594	A2	1	1	115.59
88	2	2	21	1.0585	A2	1	1	115.74
89	3	1	20	1.0546	A1	1	1	116.01
90	4	0	16	1.0539	A1	2	2	116.14
91	4	0	16	1.0539	A2	1	1	116.54
92	2	3	11	1.0486	A1	2	2	117.07
93	1	1	30	1.0469	A1	2	2	117.38
94	2	3	11	1.0486	A2	1	1	117.48
95	1	1	30	1.0469	A2	1	1	117.79
96	4	1	6	1.0427	A1	2	2	118.15
97	1	4	6	1.0427	A1	1	1	118.15
98	4	1	6	1.0427	A2	1	1	118.57
99	0	4	17	1.0375	A1	2	2	119.12
100	0	4	17	1.0375	A2	1	1	119.54
101	4	1	9	1.0211	A1	3	2	122.32
102	1	4	9	1.0211	A1	2	1	122.32
103	4	1	9	1.0211	A2	1	1	122.77
104	1	4	9	1.0211	A2	1	1	122.77
105	4	0	19	1.0041	A1	1	1	125.96
106	0	4	20	0.9873	A1	10	11	129.92
107	1	2	29	0.9853	A1	1	1	130.41
108	0	4	20	0.9873	A2	5	6	130.45
109	1	2	29	0.9853	A2	1	1	130.95
110	1	0	34	0.9753	A1	1	1	133.00
111	2	0	32	0.9700	A1	1	1	134.49
112	2	0	32	0.9700	A2	1	1	135.08
113	4	0	22	0.9538	A1	2	2	139.37
114	4	0	22	0.9538	A2	1	1	140.05
115	3	2	19	0.9454	A1	1	1	142.21

Table A-1 (cont'd)

Beta"-alumina, Co Radiation, No absorption, Cauchy P.W. = 0.25 at 40 deg.

Sort No.	h	k	l	d Space	Wave length	Rel. I(obs)	Rel. I(cal)	Two Theta
116	0	0	36	0.9403	A1	1	1	144.08
117	2	1	31	0.9387	A1	4	4	144.67
118	0	0	36	0.9403	A2	1	1	144.85
119	2	1	31	0.9387	A2	2	2	145.46
120	3	1	26	0.9366	A1	2	2	145.49
121	3	3	0	0.9357	A1	1	0	145.86
122	2	2	27	0.9350	A1	4	4	146.13
123	3	1	26	0.9366	A2	1	1	146.30
124	0	5	10	0.9346	A1	2	2	146.30
125	2	2	27	0.9350	A2	2	2	146.96
126	0	5	10	0.9346	A2	1	1	147.13
127	2	3	20	0.9313	A1	1	1	147.65
128	2	3	20	0.9313	A2	1	1	148.51
129	5	0	11	0.9272	A1	3	2	149.46
130	0	3	30	0.9260	A1	1	1	150.00
131	3	0	30	0.9260	A1	2	2	150.00
132	5	0	11	0.9272	A2	2	1	150.38
133	1	4	18	0.9240	A1	1	1	150.93
134	4	1	18	0.9240	A1	1	1	150.93
135	3	0	30	0.9260	A2	1	1	150.94
136	0	3	30	0.9260	A2	1	1	150.94
137	3	3	6	0.9231	A1	2	3	151.40
138	0	2	34	0.9213	A1	1	1	152.26
139	3	3	6	0.9231	A2	1	1	152.39
140	2	4	1	0.9185	A1	5	5	153.74
141	4	2	2	0.9175	A1	2	1	154.29
142	1	2	32	0.9168	A1	1	1	154.67
143	2	4	1	0.9185	A2	3	2	154.82
144	4	2	2	0.9175	A2	1	1	155.40
145	2	4	4	0.9134	A1	6	4	156.60
146	2	4	4	0.9134	A2	3	2	157.83
147	3	3	9	0.9080	A1	4	4	160.19
148	3	3	9	0.9080	A2	2	2	161.66

APPENDIX B

X-RAY POWDER DIFFRACTION DATA FOR SODIUM BETA -ALUMINA

The diffraction pattern generated by Fe-filtered $Co_{K\alpha}$ radiation was calculated from the observations of Peters et al. (ref. 25).

Table B-1 - Calculated X-ray powder diffraction pattern for sodium beta-alumina*

Beta alumina, Co radiation, No absorption, Cauchy P.W. = 0.25 at 40 deg.

Sort No.	h	k	l	d Space	Wave length	Rel. I(obs)	Rel. I(cal)	Two Theta
1	0	0	2	11.2650	β	1	1	8.25
2	0	0	2	11.2650		100	100	9.11
3	0	0	4	5.6325		26	25	18.29
4	1	0	1	4.7363		1	1	21.79
5	1	0	2	4.4505		11	10	23.21
6	1	0	3	4.0710		5	5	25.40
7	1	0	4	3.6729		1	1	28.21
8	1	0	6	2.9679		1	1	35.11
9	0	0	8	2.8162		2	2	37.06
10	1	1	0	2.7970		10	9	37.33
11	1	0	7	2.6809		24	24	39.01
12	1	1	4	2.5051		17	16	41.87
13	1	0	8	2.4347		2	2	43.14
14	2	0	0	2.4223		1	1	43.37
15	2	0	1	2.4084		12	11	43.64
16	2	0	2	2.3681		5	5	44.42
17	2	0	3	2.3053		1	1	45.69
18	0	0	10	2.2530		2	2	46.82
19	1	1	6	2.2431		9	9	47.04
20	2	0	4	2.2252		3	3	47.44
21	1	0	9	2.2240		1	1	47.47
22	2	0	5	2.1335		12	10	49.61
23	1	0	10	2.0429		2	2	51.97
24	2	0	6	2.0355		15	14	52.18
25	2	0	7	1.9354		9	9	55.10
26	2	0	8	1.8364		3	3	58.34
27	1	1	10	1.7546		1	1	61.35
28	2	0	10	1.6497		2	2	65.72
29	1	0	13	1.6318		1	1	66.53
30	3	0	0	1.6148		1	1	67.32
31	0	0	14	1.6093		1	1	67.59
32	2	1	7	1.5915		10	10	68.45
33	2	0	11	1.5640		7	7	69.82

* These computations were performed by Dr. Szymanski, Mineral Sciences Laboratories, CANMET.

Table B-1 (cont'd)

Beta alumina, Co Radiation, No absorption, Cauchy P.W. = 0.25 at 40 deg.

Sort No.	h	k	l	d Space	Wave length	Rel. I(obs)	Rel. I(cal)	Two Theta
34	1	1	12	1.5589		2	2	70.09
35	3	0	4	1.5523		3	3	70.43
36	2	1	8	1.5351		2	2	71.34
37	3	0	6	1.4835		3	3	74.22
38	2	1	9	1.4779		1	1	74.55
39	2	1	10	1.4210		2	2	78.09
40	2	0	13	1.4095		11	11	78.85
41	2	2	0	1.3985		19	20	79.59
42	2	2	2	1.3878		2	2	80.33
43	2	2	4	1.3573		3	2	82.52
44	2	0	14	1.3404		9	9	83.79
45	2	1	13	1.2587		1	1	90.66
46	2	2	8	1.2526		1	1	91.22
47	3	1	7	1.2399		4	4	92.42
48	3	0	12	1.2243		1	1	93.96
49	4	0	1	1.2094	A1	1	1	95.39
50	4	0	5	1.1696	A1	1	1	99.77
51	4	0	6	1.1527	A1	1	1	101.79
52	4	0	7	1.1335	A1	1	1	104.20
53	2	0	18	1.1120	A1	1	1	107.10
54	1	0	20	1.0972	A1	1	1	109.21
55	3	1	13	1.0619	A1	1	1	114.77
56	2	2	14	1.0556	A1	2	1	115.85
57	2	2	14	1.0556	A2	1	1	116.24
58	3	2	7	1.0505	A1	2	2	116.73
59	3	2	7	1.0505	A2	1	1	117.14
60	1	0	21	1.0475	A1	1	1	117.28
61	1	1	20	1.0449	A1	1	1	117.74
62	4	0	11	1.0425	A1	2	2	118.18
63	4	0	11	1.0425	A2	1	1	118.60
64	4	1	4	1.0390	A1	1	1	118.83
65	4	1	4	1.0390	A2	1	1	119.25
66	4	1	6	1.0176	A1	2	2	123.04
67	4	1	6	1.0176	A2	1	1	123.50
68	4	0	13	0.9927	A1	4	4	128.58
69	4	0	13	0.9927	A2	2	2	129.09
70	4	0	14	0.9677	A1	4	4	135.13
71	4	0	14	0.9677	A2	2	2	135.73
72	2	1	20	0.9595	A1	1	1	137.58
73	2	1	20	0.9595	A2	1	1	138.22
74	3	1	17	0.9435	A1	1	1	142.88
75	2	0	22	0.9433	A1	1	1	142.98

Table B-1 (cont'd)

Beta alumina, Co Radiation, No absorption, Cauchy P.W. = 0.25 at 40 deg.

Sort No.	h	k	l	d Space	Wave length	Rel. I(obs)	Rel. I(cal)	Two Theta
76	0	0	24	0.9387	A1	1	1	144.66
77	3	2	13	0.9356	A1	1	1	145.91
78	2	2	18	0.9327	A1	2	2	147.09
79	2	2	18	0.9327	A2	1	1	147.93
80	5	0	7	0.9278	A1	2	2	149.20
81	5	0	7	0.9278	A2	1	1	150.11
82	2	1	21	0.9257	A1	2	2	150.16
83	3	0	20	0.9239	A1	2	2	150.99
84	2	1	21	0.9257	A2	1	1	151.10
85	3	0	20	0.9239	A2	1	1	151.96
86	4	1	12	0.9212	A1	1	1	152.33
87	3	3	4	0.9198	A1	1	1	153.03
88	3	3	4	0.9198	A2	1	1	154.08
89	5	0	8	0.9162	A1	1	1	154.99
90	3	1	18	0.9159	A1	1	1	155.18
91	4	2	0	0.9155	A1	1	0	155.37
92	4	2	1	0.9148	A1	4	3	155.80
93	4	2	1	0.9148	A2	2	2	156.98
94	4	2	2	0.9125	A1	1	1	157.16
95	4	2	3	0.9088	A1	2	2	159.61
96	4	2	3	0.9088	A2	1	1	161.04
97	3	3	6	0.9049	A1	3	3	162.61
98	5	0	9	0.9036	A1	1	1	163.70
99	3	3	6	0.9049	A2	2	2	164.31

OPINION POLL

The opinion of concerned readers may influence the direction of future CANMET research.

We invite your assessment of this report - No._____

Is it useful?	Yes_____	No_____
Is it pertinent to an industry problem?	Yes_____	No_____
Is the subject of high priority?	Yes_____	No_____

Comments_____

_____

_____

Please mail to: CANMET Editor, EMR, 555 Booth Street,
Ottawa, Ontario, K1A 0G1

A complimentary copy of the CANMET REVIEW describing CANMET research activity will be sent on request.

CANMET REPORTS

Recent CANMET reports presently available or soon to be released through Printing and Publishing, Supply and Services, Canada (addresses on inside front cover), or from CANMET Publications Office, 555 Booth Street, Ottawa, Ontario, K1A 0G1:

Les récents rapports de CANMET, qui sont présentement disponibles ou qui le seront bientôt peuvent être obtenus de la direction de l'Imprimerie et de l'Edition, Approvisionnements et Services Canada (adresses au verso de la page couverture), ou du Bureau de vente et distribution de CANMET, 555, rue Booth, Ottawa, Ontario, K1A 0G1:

79-8 Flotation techniques for producing high-recovery bulk Zn-Pb-Cu-Ag concentrate from a New Brunswick massive sulphide ore; A.I. Stemerowicz and G.W. Leigh;
Cat. No. M38-13/79-8, ISBN 0-660-10448-2; Price: $8.00 Canada, $9.60 other countries.

79-10 A comparative study of lightweight aggregates in structural concrete; H.S. Wilson;
Cat. No. M38-13/79-10, ISBN 0-660-10449-0; Price: $2.00 Canada, $2.40 other countries.

79-11 CANMET's rock mechanics research at the Kid Creek mine; D.G.F. Hedley, G. Herget, P. Miles and Y.S. Yu;
Cat. No. M38-13/79-11, ISBN 0-660-10472-5; Price: $3.50 Canada, $4.20 other countries.

79-17 Rapid chromatographic procedure for characterizing hydrocarbons in synthetic fuel naphtha; A.E. George, G.T. Smiley and H. Sawatzky;
Cat. No. M38-13/79-17, ISBN 0-660-10428-8; Price: $2.75 Canada, $3.30 other countries.

79-18 Influence of flue temperature and coal preparation on coke quality in 460-mm technical scale coke oven; J.F. Gransden and W.R. Leeder;
Cat. No. M38-13/79-18, ISBN 0-660-10441-5; Price: $1.50 Canada, $1.80 other countries.

79-20 Effect of hydrocracking on the distribution of nitrogenous components in Athabasca bitumen; H. Sawatzky, J.E. Beshai, G.T. Smiley and A.E. George;
Cat. No. M38-13/79-20, ISBN 0-660-10442-3; Price: $1.25 Canada, $1.50 other countries.

79-25 CANMET review 1978-79; Staff of CANMET;
Cat. No. M38-13/79-25, ISBN 0-660-10522-5; Price: $4.25 Canada, $5.10 other countries.

79-28 Sulphur concrete and sulphur infiltrated concrete: Properties, applications and limitations; V.M. Malhotra;
Cat. No. M38-13/79-28, ISBN 0-660-10469-5; Price: $2.25 Canada, $2.70 other countries.

79-29 Geological disposal of high-level radioactive wastes; D.F. Coates, G. Larocque and L. Geller; (Policy paper);
Cat. No. M38-13/79-29, ISBN 0-660-10523-3; Price: $1.50 Canada, $1.80 other countries.

79-30 In situ testing for concrete strength; V.M. Malhotra and G.G. Carette;
Cat. No. M38-13/79-30, ISBN 0-660-10506-3; Price: $1.75 Canada, $2.10 other countries.

79-31 Superplasticizers: Their effect on fresh and hardened concrete; V.M. Malhotra;
Cat. No. M38-13/79-31, ISBN 0-660-10530-6; Price: $2.00 Canada, $2.40 other countries.

79-32 Concrete made with supplementary cementing materials; E.E. Berry;
Cat. No. M38-13/79-32, ISBN 0-660-10470-9; Price: $2.25 Canada, $2.70 other countries.

79-33 Lightweight aggregates: Properties, applications and outlook; H.S. Wilson;
Cat. No. M38-13/79-33, ISBN 0-660-10482-2; Price: $2.25 Canada, $2.70 other countries.